Active fault scarps in southern Malawi and their implications for the distribution and evolution of strain in amagmatic continental rifts

L. N. J. Wedmore[1], J. Biggs[1], J. N. Williams[2], Å. Fagereng[2], Z. Dulanya[3], F. Mphepo[4], H. Mdala[4]

[1]Department of Earth Sciences, University of Bristol, UK.

[2]School of Earth and Ocean Sciences, Cardiff University, UK

[3]Geography and Earth Sciences Department, University of Malawi, Zomba, Malawi

[4]Geological Survey Department, Mzuzu Regional Office, Mzuzu, Malawi

Corresponding author: Luke Wedmore (luke.wedmore@bristol.ac.uk)

Key Points:

- In the Zomba Graben, southern Malawi, we identify 5 subparallel, 10-50 km long, 3-20 m high, previously unrecognised fault scarps.
- ~75% strain since rift initiation was focussed on the border faults, but the intra-rift strain has increased by ~25% during this period.
- The Zomba Graben is a zone of relatively high seismic hazard linking Lake Malawi to the Urema Graben in Mozambique.

Abstract

The distribution of deformation during early stages of continental rifting is an important constraint on our understanding of continental breakup. Early stage rifting is typically considered to be dominated by slip along rift border faults. The subsequent transition to focussed extension on axial segments is thought to require thinned crust and active magmatism. Here we study high resolution satellite data of the Zomba Graben in southern Malawi, an amagmatic rift with a short (<10-5 Ma) history of extension, but little prior evidence of active faulting. We discover active fault scarps that probably represent late-Quaternary activity in the graben and represent a previously unrecognised seismic hazard. By comparing total fault displacements since rift initiation with the heights of newly identified, recently formed fault scarps, we constrain the spatial evolution of strain through the early stages of continental rifting. Whereas 75 ± 18 % of the total extension was accommodated by slip along border faults, displacement along three intra-rift fault scarps demonstrate that current extension is distributed throughout the graben. The border faults remained active throughout the period of rifting, but displacement on the intra-rift faults has increased from 25 ± 8 % of the total extensional strain, to 50 ± 25% of the recent extensional strain. Previous models of the East African Rift suggest that the transition from border fault dominated to axial strain is driven by fluids or runaway lithospheric thinning. Our observations demonstrate that significant intra-rift strain can occur in thick continental lithosphere with no evidence for magmatic fluids.

Plain Language Summary

When continents begin to stretch, individual faults host earthquake that incrementally accumulate slip to eventually form a rift valley. To estimate earthquake hazard, it is

important to understand where these faults are located, and how much stretching they accommodate. We analyse faults in the Zomba Graben, a young rift in southern Malawi using high-resolution satellite data. Since the rift formed, most of the deformation has occurred at the edges of the rift valley. In contrast, steep scarps, indicate that more recent earthquakes have occurred at both the edges and the middle of the rift valley. This shift occurs much earlier than previously thought, and is not associated with volcanic fluids weakening the Earth's crust as suggested by existing models. Instead, the distribution of faults, and hence of earthquakes, is likely due to weaknesses in the middle and lower parts of the Earth's crust.

1. Introduction

The development and interaction of faults dominate the early stages of continental rifting and contribute to the eventual breakup of continental lithosphere (Cowie et al. 2005; Ebinger and Scholz, 2012). Current conceptual models suggest that rifting is initially dominated by activity on border faults (Ebinger, 2005, Muirhead et al 2019). During these early stages, intra-basin faulting is limited to small-displacement faults that accommodate flexure, and strain only begins to migrate to the rift interior when magmatic intrusions weaken the lithosphere and cause runaway thinning (Buck, 2004; Ebinger, 2005). However, because these later phases of magmatic rifting are associated with changes in sedimentation, fault activity, and volcanism, patterns of intra-basin faulting generated during earlier stages of rifting are typically obscured.

The overall mode of a rift (e.g. narrow vs wide *sensu* Buck 1991) is thought to be predominately controlled by the interplay between Moho temperature, crustal thickness, and strain rate (Buck, 1991; Huismans and Beaumont, 2007). In contrast, the surface expression of a rift - whether faults form symmetric grabens or asymmetric half-grabens, and the length, orientation and segmentation of major faults - is controlled by crustal rheology (Huismans and Beaumont, 2007; Hodge et al., 2018). Within the East African Rift system, there is evidence for both narrow and wide rift modes (*sensu* Buck, 1991; Ebinger and Scholz, 2012), symmetric and asymmetric grabens (Ebinger et al, 1999; Lao Davila et al, 2015) and a range of relationships between fault strike, metamorphic foliation, and regional stresses (Hodge et al., 2018; Williams et al., *in revision*). The lack of constraints on strain distribution, geochronology and geophysical properties in East Africa makes it challenging to ascertain the relative roles of shallow crustal rheology, heatflow, crustal thickness and finite strain in shaping the geometry of incipient rift basins.

To investigate the geometry and strain distribution within a youthful rift, we analyse the geomorphic signature of an active normal fault array in the Zomba Graben, which is at the southern end of the incipient, amagmatic Malawi Rift. The graben is dominated by a west-dipping border fault, but we also find evidence for both syn- and antithetic normal faults in its hanging wall. As well as the prominent border faults, we use geomorphic analysis of high-resolution topographic data to detect five previously unrecognised active fault scarps. We compare footwall escarpments that are representative of the long-term pattern of strain in the graben, with fault scarps that represent more recent displacements. This analysis is then used to address how and when rift-related deformation is distributed between the border faults and faults within the rift interior. Our findings have implications for our understanding of the evolution of strain in the early stages of continental rifting and the associated seismic hazard.

2. Tectonic and Geological Setting

2.1. The Malawi Rift

The ~ 900 km long Malawi Rift System is located at the southern end of the largely amagmatic western branch of the East African Rift System (EARS; Ebinger et al., 1987; Figure 1). The rift along Lake Malawi is defined by a series of asymmetric half-grabens with segmented border faults that offset Proterozoic medium to high grade metamorphic rocks with fabrics formed in multiple Precambrian orogenic events (Fritz et al., 2013). The border faults are ~120 km long with up to ~ 6 km of throw related to the current rift regime (Contreras et al., 2000; Lao-Davila et al., 2015). The locations of faults in Lake Malawi are well constrained by a number of seismic surveys carried out in the lake (Scholz and Rosendahl, 1988; Scholz, 1995; Lyons et al., 2011; Shillington et al., 2016) as well as a recent network of lake bottom and onshore seismometers in northern Malawi and Tanzania (Shillington et al., 2016; Accardo et al., 2018). These seismic surveys, along with the 2009 Karonga earthquake sequence that occurred within the hanging wall of the rift-bounding Livingstone Fault, indicate that both rift border and intrabasinal faults are currently active at the northern end of the Malawi Rift (Biggs et al 2010, McCarntney and Scholz 2017, Gaherty et al 2019). Active faulting is also occurring at the southern end of the lake, as demonstrated by the M_w 6.1 1989 Salima Earthquake (Jackson and Blenkinsop 1993).

Rifting within the western branch of the EARS is thought to have initiated in the Oligocene (~25 Ma; Roberts et al., 2012). Low-temperature cooling ages from the northern basin of Lake Malawi indicates that regional scale cooling, associated with the onset of rifting, commenced at ~23 Ma (Mortimer et al., 2016), and thus earlier than previously proposed age of ~9 Ma based on radiometric dating of volcanic and volcanoclastic deposits from northern Malawi (Ebinger et al., 1993). The age of the rift in central and southern Malawi is, however, poorly-constrained. A 4.6 Ma age has been proposed for the onset of sediment accumulation in Lake Malawi's central basin (~350 km to the north of the Zomba Graben), from extrapolating the average rates of sediment accumulation in ~1.3 Ma drill core (Lyons et al 2015) to the entire sedimentary sequence (McCartney and Scholz 2016). This would suggest a gradual southward propagation of the rift (Ebinger et al., 1987; Contreras et al., 2000), which is consistent with sediment thickness and footwall topography decreasing from north to south within Lake Malawi (Specht and Rosendahl, 1989; Flannery and Rosendahl, 1990; Lao Davila et al., 2015). An alternative hypothesis is that the onset of extension is uniform along the Malawi Rift, but the extension rate is faster in the northern part of the rift because the Euler pole of the plates is located south of the Malawi Rift (Calais et al., 2006; Saria et al., 2014; Stamps et al., 2018). Although there are currently few constraints on the age of the EARS to the south of Lake Malawi (Dulanya et al 2017), we consider it unlikely that extension initiated in this region prior to the onset of sedimentation in Lake Malawi. This places an approximate maximum age of the rifting in the Zomba Graben as the mid-Miocene to early-Pliocene.

The onshore rift south of Lake Malawi consists of three linked half-grabens (Figure 1, Williams et al, in revision). The border faults have escarpment heights of <1000 m, and so are less prominent than those within the lake (Lao-Davila et al., 2015). The initiation and accumulation of displacement on these faults is thought to have led to Lake Malawi becoming externally drained via the River Shire, which links the lake to the Zambezi River (Dulanya, 2017; Figure 1). The NW-SE trending Makanjira graben contains two known active faults: the ~55 km long Malombe fault, and the ~110 km long Bilila-Mtakataka fault, a possible source of the 1989 M_w6.1 Salima Earthquake (Jackson and Blenkinsop, 1993; Hodge et al., 2018; 2019). Immediately south of the Makanjira graben lies the Zomba Graben, which is the focus of this study and described in more detail in section 2.2. To the south of the Zomba Graben, in the middle Shire Valley, the river drops by ~ 380m in elevation with no evidence of active faulting (Dulanya, 2017; Figure 1). The NW-SE trending Lower Shire graben lies ~60 km further south and is a reactivated Karoo-age basin bounded to the east by the 85 km long active Thyolo fault (Figure 1b; Hodge et al., 2019). The EARS continues south into the Urema Graben, the site of repeated seismic activity following the 2007 M_w7.0 Machaze earthquake (Lloyd et al, 2019; Copley et al., 2012).

2.2. The Zomba Graben

The Zomba Graben is a NE-SW trending segment of the onshore Malawi Rift where the dominant structure is the NW-dipping Zomba fault. The Zomba Graben has traditionally been considered a half-graben similar to those in Lake Malawi (e.g. Ebinger et al., 1987), but Lao Davila et al. (2015) map it as a ~50 km wide full-graben, bounded to the west by the E-dipping Lisungwe fault.

The topography of the Zomba Graben is influenced by structures within the basement complex, which comprises Proterozoic metamorphic rocks of the Southern Irumide Belt and subsequent intrusions. On the western side of the rift, the mountainous Kirk range is composed of metasedimentary schists, paragneisses and granulites, and contrasts with the lower elevation eastern side, which is composed of meta-igneous charnockitic granulites (Figure 2; Bloomfield and Garson, 1965). Syn and postkinematic intrusions form local regions of high topography. The most notable of these are the Proterozoic Chingale Ring

Complex, and the Upper Jurassic-Lower Cretaceous Chilwa Alkaline Province, which includes the Zomba Massif quartz-syenite and granite intrusion (Bloomfield 1965, Eby et al 1995).

Despite the apparent presence of border faults within the Zomba Graben, little is known about the distribution of faulting in the region and the way in which strain is distributed. A set of escarpments in the centre of the graben that offset fluvio-lacustrine sediments have been variously mapped as ‘terrace features' (Bloomfield, 1965; Figure 2), active fault scarps (Dixey, 1926) and inactive late-Jurassic or early Cretaceous faults (Dixey, 1938).

3. Active faults within the Zomba Graben

Within Malawi, faults have been identified as active based on the presence of a continuous, steep scarp at the base of the footwall at the surface (Jackson and Blenkinsop, 1997; Hodge et al., 2018; 2019). Observations of soft hanging wall sediments, preserved uplifted river terraces in the footwall, and knickpoints in streams close (within <100 m) to the fault scarps were also used as evidence to confirm the faults are active (Jackson and Blenkinsop, 1997). These criteria have been used prior to this study to identify three active faults south of Lake Malawi but outside the Zomba Graben: The Bilila Mtakataka, Malombe and Thyolo faults (Figure 1c; Hodge et al., 2019). As no active faults had previously been identified in the Zomba Graben, geological maps were used to first identify faults where Bloomfield (1965) identified tertiary-recent hanging wall sediments (Figure 3a). The detailed topographic analysis described below was then used to determine whether a fault has formed an active fault scarp, in which case the fault would be considered currently active. We supplement these observations with fieldwork, from a 6-week campaign in 2018.

3.1. Topographic analysis to assess fault activity

We used a TanDEM-X digital elevation model (DEM) of the Zomba Graben to identify and analyse fault scarps and the river channels that cross them (Figure 3). TanDEM-X DEMs have a horizontal resolution of 12.5 m and an absolute vertical mean error of ± 0.2 m (RMSE < 1.4 m; Wessel et al., 2018), which is sufficient for measuring the meter-scale fault scarps in the Zomba Graben. We consider the presence of a linear scarp coinciding with changes in channel incision and width, and hanging wall sediment deposition, as evidence for active faulting during the current rifting episode (Figure 3).

We produced slope maps from the DEM by calculating the scalar magnitude of the slope derivative using the grdgradient tool in the Generic Mapping Tools routines (Wessel and Smith, 1998; Figure 3b) and use these maps to identify the location of the active fault scarps. We noted any gaps in the scarps, or peaks and troughs in the displacement profiles, that may be indicative of fault segmentation (following Hodge et al., 2018). We extracted 500 m long fault-perpendicular topographic profiles every 12 m, and stacked them at 100 m intervals. The stacking has the effect of removing short-wavelength random topographic features not related to the fault such as local sedimentation and erosion or human settlements and vegetation close to the fault. The surface offset was calculated by fitting regression lines to the footwall and hanging wall topography of the stacked profiles, and measuring the vertical difference between the extrapolated regression lines at the point of maximum steepness on the scarp (Avouac, 1993; Figure 4a). To estimate the uncertainty, we applied a Monte Carlo approach by selecting 10,000 random subsets of points from the footwall and hanging wall, and allowing the exact location of the fault to vary. The variation between profiles is due to a combination of differential geomorphic degradation of the fault scarp and variation in fault offset that forms during an earthquake. Example profiles for each fault are shown in Figure 4a. We filter the resulting measurements along strike using a 3 km wide moving median (Hodge et al., 2018; 2019).

Rivers that cross normal faults record information about the timing and magnitude of active faulting in their long profile (i.e. their change in elevation with distance along the channel) and can be used as an indicator of fault activity in regions where the location of active faults is poorly constrained (Boulton and Whittaker 2009). We extracted long profiles of rivers in the Zomba Graben with a drainage area greater than 6,000 m^2 using TopoToolbox (Schwanghart and Scherler, 2014). We identified changes in channel steepness that are evidence of perturbations to the power-law relationship, $S = k_{sn} A^{-\theta ref}$, between local channel gradient, S, and upstream drainage area, A, in detachment limited rivers (Whipple and Tucker 1999). We use a reference concavity index, $\theta_{ref} = 0.45$ to calculate a normalised channel steepness index value, k_{sn}, using the 12.5 m resolution DEM, thus facilitating a comparison between streams with a large range of drainage areas (Wobus et al., 2006). Consistent along-strike increases in K_{sn} suggest a perturbation of the stream power law due to changes in uplift rates caused by active normal faulting (Wobus et al., 2006; Figure 3d).

3.2. *Description of fault scarps*

Based on the topographic analysis we found evidence for five active fault scarps within the Zomba Graben that we subsequently confirmed during a 6-week field campaign in 2018. In this section, we describe the tectonic geomorphology and field observations of the five faults which includes two border faults, Zomba and Lisungwe, and three intrarift faults, Chingale Step, Mlungusi and Mtsimukwe. For each fault, we report the dimensions of the fault scarps discovered at the base of footwall escarpments (all measurements are listed in

Table S1-S11 in the supplementary material), and describe the other features that led us to conclude they are active. The measurements are shown in Figure 5 and summarised in Table 1.

The NW-dipping Zomba fault borders the eastern side of the Zomba Graben and has a ~50 km long escarpment with an active fault scarp at the base (Figure 5a and Figure S1). The mean height of the fault scarp is 15.6 ± 5.2 m (Figures 4a & 5a) and normalised channel steepness values (K_{sn}) increase where rivers cross the fault (Figure S1d). Higher K_{sn} values 3-4 km into the hanging wall at the northern end of the fault are associated with the distal edges of alluvial fans sourced from the Zomba Plateau (Figure S1d). The scarp is noticeably steeper adjacent to the Zomba Plateau and a ~2 km step to the north-west occurs at the northern end of the fault in front of the Zomba Plateau (Figure S1b-c). At the northern end of the fault, triangular facets were observed in the field (Figure 6a). Large alluvial fans in the hanging wall are composed of material derived from the Zomba Plateau and appear to have been offset by the fault (Figure 6b). In the middle of the fault, a ~17 m high fault scarp was observed during fieldwork (Figure 6c). At the base of the scarp, a zone of highly fractured gneiss was observed, consistent with a fault zone (Figure 6d).

The NW-dipping Chingale Step fault (Figures 4a & 5b and Figure S2) is located approximately 10 km into the hanging wall of the Zomba fault and has formed a ~40 km long composite scarp with evidence for multiple offsets (Figure 4a and Figure S2) and two segments (Figure 5b and Figure 7). Although the average scarp height along the whole fault is 19.6 ± 12.1 m (black line Figure 5b), the scarp in the northern segment (25.2 ± 11.7 m) is higher on average than the scarp in the southern segment (15.1 ± 10.6 m). In contrast, the height of the lowermost offset is approximately constant along the entire length of the fault (5.7 ± 2.5 m; red line in Figure 5b).

Where river channels cross the Chingale Step fault, K_{sn} increases (Figure S2) and the upstream long profiles are oversteepened (Figure 7c-d and Figure S3). Plotting the elevation of the top of the oversteepened reaches shows two fault segments separated by a zone of linkage (Figure 7). The river channel within this linkage zone shows two knickpoints, likely related to the separate initiation of faulting of the southern and northern segments (Figure 7c). The consistent offset measured across the lowermost fault scarp (red line in Figure 5b) suggests that these segments have linked in the time since the active fault scarp begun to be preserved, and are now operating as a single fault. A scarp was visible along all sections visited, with a zone of fault gouge and fractured basement rocks visible at the base of the fault scarps in exposed stream beds (Figure 8). At the Kalira river site, the fault surface itself was visible with a polished surface and slickensides (Figure 8). The composite scarp was not visible in the field, although most accessible locations were on the southern end of fault where the difference between the total scarp and the lowermost scarp was smaller than along the northern segment of the fault.

The SE-dipping Mlungusi fault has formed a ~20 km long scarp in the centre of the Zomba Graben (Figures 4a & 5c) and has a mean scarp height of 6.9 ± 3.1 m. The slope map shows a prominent scarp along the entire length of the fault (Figure S4), whereas K_{sn} values are only elevated in the centre of the fault (Figure S4d). The Shire River crosses the southern end of the Mlungusi fault, where it changes from a wide, meandering channel with a floodplain in the hanging wall, to a narrow, incised channel with an associated set of rapids as it crosses into the footwall (Figure 9). Along strike from this location, a steep fault scarp was observed in the field (Figure 9b) which has offset alluvial-lacustrine deposits found on the floor of the graben. The central segment of the fault scarp is covered by lacustrine beach deposits characterised by rounded to subrounded pebbles within a clast-supported sandy matrix (Figure 9b). Long-term footwall uplift has led to drainage reorganisation as rivers draining into the axial Mtsimukwe River in the footwall of the Mlungusi fault are restricted to the western side of the channel, distal to the fault (Figure S4d).

The E-dipping Mtsimukwe fault has formed a ~13 km long scarp trending ~N-S (Figures 4a 5d). The mean scarp height is 3.6 ± 0.7 m. The slope map shows that the fault scarp is best preserved in the central part of the fault except a ~2 km long section where the fault intersects a road (Figure S5b). The streams that cross the fault show a small increase in K_{sn} value, with the largest increase in centre of the fault, but there is no evidence of segmentation (Figure S5).

The E-dipping Lisungwe fault is the western border fault of the Zomba Graben (Figure 2 and Figure 5e). High slope values have a linear trend aligned with an increase in K_{sn} in the streams that cross the escarpment (Figure S6). The mean offset across the late-Quaternary fault scarp is 10.0 ± 6.7 m (Figures 4a & 5e). No fieldwork was conducted on the Mtsimukwe and Lisungwe faults fault due to access reasons, but the remote sensing observations described above and seen in Figure S5 and Figure S6 are similar to the observations on faults (e.g. Zomba, Chingale Step and Mlungusi faults) where fieldwork was able to confirm the evidence gained remotely.

3.3. Fault Kinematics and Extension Direction

The extension direction within the Zomba Graben is approximately NW-SE, as inferred from measurements of slickensides along the Chingale Step Fault (Figure 8b-d; plunging 52°

towards 301°) and elsewhere in the graben (Bloomfield, 1965; Chorowicz and Sorlien, 1992). The trend of these slickensides is orthogonal to the surface traces (015 ± 11°) of the 5 faults, indicating dip-slip displacement. This contradicts previous rift-wide estimates of NE-SW extension (Delvaux and Barth, 2010; Figure 1). However, these estimates likely reflect that normal faulting events in the Malawi Rift are approximately purely dip-slip despite regional changes in fault strike (Williams et al., *in review*), as also indicated by the 2009 Karonga Earthquakes (Biggs et al., 2010), the 1989 Salima earthquake (Jackson and Blenkinsop, 1993), and a M_w=5.6 earthquake in March 2018 (red focal mechanism in Figure 1b). Previous rift-wide estimates of NE-SW extension do therefore not necessarily apply to the Zomba Graben.

3.4. Distribution of contemporary strain in the Zomba Graben

We found evidence for five active faults within the Zomba Graben. The largest fault scarp was found along the Chingale Step fault, which is located in the hanging wall of the border fault. The distribution of fault scarps within the graben is a notable feature. The across strike spacing between the active faults is approximately 10-15 km and the height of each fault scarp ranges between ~4 and ~20 m. Thus, the strain within the Zomba Graben over the time period that the active fault scarps have formed is not localised on a single major border fault but instead distributed across the width of the rift. To explore whether this pattern of distributed faulting is a long-lived feature of the rift, we make an assessment of the longer term deformation in the region and compare the patterns of strain over both timescales.

4. Fault activity since the onset of rifting

All five faults have formed active fault scarps at the base of a larger footwall escarpment, which represents the longer-term topographic record of faulting. In this section, we measure this longer-term record of faulting which allows us to compare the distribution of strain associated with the active fault scarps (Section 3) with the strain in the Zomba Graben since the onset of rifting. We consider the height of the footwall escarpments to represent the minimum throw on each fault since the onset of rifting, as erosion of the footwall and deposition of sediment in the hanging wall have likely reduced the total faulted relief. As before, we extracted fault-perpendicular topographic profiles, but in this case, we stacked in 1 km wide bins and the profiles were 6 km long. As progressive fault slip results in rotation of the footwall block (Wernicke and Axen, 1988), we used the maximum elevation of the footwall within 3km of the fault (relative to the base of the scarp), rather than fitting regression lines to the footwall and hanging wall slopes (see Figure 4b for examples from the centre of each fault).

We assume that there was little significant relief across the escarpment at the onset of faulting and that there is no spatial variation in erosion and deposition rates across the Zomba Graben. Neither of these assumptions apply to areas that have experienced local intrusions into the Precambrian basement, therefore we disregard measurements made in these areas. To test these assumptions, we calculate the local relief: the range of topography within a 1 km window. Although local relief is affected by basin infilling, low values of local relief both inside and outside the graben would suggest a lack of pre-existing topography, and spatially uniform values of local relief in the hanging wall and footwall of the faults would suggest a lack of significant erosion or sedimentation. Meanwhile, low values of local relief are thought to be consistent with low erosion rates (Montgomery and Brandon, 2002). To assess the depth of hanging wall sediments we used logs from drinking water boreholes described on the geological maps (Figure 2a; Bloomfield 1965).

4.1. Footwall escarpments in the Zomba Graben

The most prominent footwall escarpment in the Zomba Graben is associated with the Zomba fault. The mean relief of the footwall of the Zomba fault is 326 ± 113 m (Figure 5a). The Zomba Plateau lies to the north of the fault, and the footwall here is about 1 km higher than in the basement gneisses to the south. As the Zomba Plateau has a higher elevation than the surrounding landscape, we suspect it violates our assumption of no significant topography prior to rifting hence we do not include it in our measurement of the mean footwall uplift.

Along the Chingale Step fault, the mean height of the footwall escarpment is 84 ± 18 m (Figure 5b; excluding measurements associated with pre-existing topography from the Chingale Ring Structure and the Chinduzi Hill nepheline-syenite province; Figure S2). Boreholes drilled on the hanging wall reached depths of 41.5 m and 49.3 m without reaching basement rock (Figure S2; Bloomfield, 1965).

The mean height of the footwall of the Mlungusi fault is 19 ± 5 m (Figure 5c). The low topographic expression of this fault may be due to higher sedimentation rates within the centre of the graben as no footwall bedrock is mapped on the geological maps (Figure 2a). However, during fieldwork, bedrock was observed in the footwall of the fault in all locations visited, shown in Figure 19.

The mean height of the footwall along the Mtsimukwe fault is 38 ± 12 m (Figure 5d). The footwall of the fault is made up of Proterozoic gneisses, and two boreholes drilled through the hanging wall sediments in 1954 (see Figure S5d for locations) penetrated the basement gneisses at depths less than 37 m (Bloomfield, 1965).

The Lisungwe fault, the western border fault of the Zomba Graben, is divided into two segments separated by an area of marble and metadolomite within the basement gneiss. However, this segmentation visible in the surface trace of the fault is only weakly visible in the height of the footwall escarpment. The footwall escarpment is 277 ± 76 m high (Figure 5e) with Tertiary-recent sediments in the hanging wall (Figure S6b-f). As the fault is located within the topography of the Precambrian Kirk Range, we removed the pre-existing topographic signal by differencing the long-wavelength topography (calculated using a low-pass Gaussian spatial filter where 6σ = 50km) and the present-day topography. This residual relief picks out the high frequency fault-related topography, which is identified by the sharp elevation contrast between the footwall and the back-tilted hanging wall block, but does not significantly affect the estimated height of the footwall escarpment (Figure S6g-h).

5. Strain distribution across the Zomba Graben

We calculate the cumulative strain since: i) the onset of faulting; and ii) since the formation of the fault scarps (assuming an approximately uniform age of the fault scarps) which allows us to assess any changes in the relative distribution of strain across the rift through time.

We calculate finite strain across the Zomba Graben using the England and Molnar (1997) adaptation of the Kostrov (1974) expression of strain rate:

$$\bar{\varepsilon}_{ij} = \frac{1}{2a}\sum_{k=1}^{k}\frac{L^k\bar{s}^k}{\sin\vartheta^k}\left(\hat{u}_i^k\hat{n}_j^k + \hat{u}_j^k\hat{n}_i^k\right) \qquad (1)$$

where a is the surface area of the region, L^k is the length of fault k in that region, s^k is the slip of fault k in that region, ϑ^k is the dip of fault k, $\hat{u}^k$ is a unit vector in the direction of slip and $\hat{n}^k$ is a unit vector normal to the fault plane. The advantage of this adaption is that it is independent of seismogenic thickness or shear modulus. We assume pure dip-slip faults that strike parallel to each other (see section 3.3), such that ε_{22} is equal to zero, and ε_{11} is perpendicular to the mean strike of the faults. The only unknown term is fault dip, for which we assume an Andersonian value of 60°, although using a randomly selected fault dip, within the usual range for normal faults (45°-60°; Collettini and Sibson 2001), produces similar results (Figure S7). We calculated the strain within 5 km (across strike) by 50 km (along strike) rectangular boxes with long axes orientated 100°.

We find differences between the distribution of strain since the onset of faulting and strain over the time period since fault scarps have been preserved (Figure 10). 75 ± 18 % of strain since the onset of faulting is focussed on the border faults (Zomba and Lisungwe faults; Figure 10b). The relief demonstrates that significant motion has occurred on both these faults, but the graben is asymmetric, with 55 ± 16 % of the strain in the region of eastern border fault (the Zomba fault), and 19 ± 3 % of strain across the western border fault (Lisungwe fault; Figure 10b) with the remaining strain accommodated on intrabasin faults. Although the Zomba and Lisungwe faults only partially overlap across strike, which may indicate they initially formed as separate half-grabens, both the profiles of strain (Figure 10b-c) and topography (Figure 2c) suggest that the Zomba Graben is a full-graben as inferred by Lao-Davlila et al. (2015). However, the eastern border fault accommodates more strain than the western border fault resulting in the asymmetric characteristics of a half-graben (Figure 10c; see also Ebinger et al., 1987).

In contrast, over the time period during which the active fault scarps have been preserved, only 50 ± 17% of strain has occurred across the two border faults (Figure 10a). In this time period, the strain dominantly occurred across the Chingale Step fault (35 ± 21 %) and the Zomba border fault (42 ± 15%), both W-dipping faults on the eastern side of the graben.

This relative change is consistent with either a decrease in the absolute strain across the Zomba border fault or an increase in the absolute strain across the Chingale Step fault, and without better time constraints, we cannot distinguish between these possibilities. However, we can conclude that a lower proportion of the strain occurred across the border fault in this period relative to the time since the onset of faulting (Figure 10b-c). The high uncertainty of the late Quaternary strain calculation is caused by high scarp height standard deviation on the Chingale Step fault, the fault which accommodates the majority of the intra-rift strain. This high standard deviation is due to segment linkage during the late Quaternary which has caused an along strike displacement profile with dual maxima (Figure 5b & 7a).

A pattern of increasing strain within the rift interior also occurs on the western side of the graben, where the proportion of strain across the Lisungwe border fault decreased from 19 ± 3% to 6 ± 2%, while the proportion across the Mlungusi fault increases from 2 ± 0.5% to 8 ± 3% and the proportion of strain across the Mtsimukwe fault remains the same within error (from 11 ± 6% to 8 ± 3%; Figure 10b-c). Although the lowest topography is currently found in the centre of the rift, the graben still retains its asymmetric character, with 78 ± 37% of the strain across W-dipping faults in the east and 22 ± 8% across E-dipping faults in the west. The distributed pattern of strain means that neither full- or half-graben models apply.

Due to a lack of geochronological dates in the Zomba Graben, we do not know the exact timing of either the onset of faulting or the age of the fault scarps. Therefore, we are unable to calculate the strain rate within the region or comment on changes in strain rate through time. As a consequence, we have limited our analysis and discussion to changes in the *relative* distribution of strain in the two different time periods identified. We discuss the validity of this comparison before commenting on the implications that can be drawn from our results for the dynamics of strain in early stage rifts.

6. Discussion and the timing of rifting in the Zomba Graben

6.1. Preservation of fault related topography since the onset of rifting

The Zomba Graben is an ideal location for using topography to study the activity of faults since the onset of rifting, as a lack of pronounced pre-existing topography is coupled with low sedimentation and erosion rates. In this section we verify that these conditions apply within the graben and show how our measurements of footwall topography allow a comparison between the activity of each fault since the onset of rifting.

In order for our measurements of footwall relief within 3 km of the surface trace of each fault to be a valid marker of faulting since the onset of rifting, we assumed that there was a lack of significant topography in the graben prior to the current rifting episode. We also assumed that rates of erosion and sedimentation across the graben are approximately uniform. If this assumption is valid, then while the absolute values of footwall topography that we measure may have been affected by erosion and sedimentation, the spatial patterns of fault activity since the onset of rifting should have been preserved. We tested these assumptions by calculating the local relief (Figure 11). In areas away from the faults and intrusions, the local relief (range of topography within a 1 km window of each point) is generally < 50 m and there is no discernible spatial pattern of different local relief values within the Zomba Graben. In the footwall of the Zomba fault, the local relief is more variable but still includes large areas where the local relief is < 50 m with similar values to the floor of the Zomba Graben. Locally high values are associated with intrusions into the Precambrian basement. The low values in the footwall of the Zomba fault (Figure 11a) and the preserved back tilted footwall topography (Figure 2c) is consistent with the preservation of a low-relief pre-rift surface that has experienced little erosion since the onset of faulting. The similarity of the low relief values between the footwall of the Zomba fault and the floor of the Zomba Graben suggests regionally low erosion and sedimentation rates, with the exception of the areas immediately surrounding the faults where values are locally elevated (Figure 11a). The median local relief in the region is 47 m (Figure 11b), which is consistent with low average erosion rates of < 1 mm yr^{-1} when compared to global comparisons of local relief and mean erosion rates (Montgomery and Brandon, 2002).

Where we were able to compile data from drinking boreholes drilled in the 1950s, basement depth in the centre of the graben (in the hanging wall of the Mtsiumkwe fault), was < 40 m, providing further evidence for low sedimentation rates since the onset of rifting. If the Mtsimukwe fault has been active since the Pliocene (~5 Ma; the minimum age of the rifting in the region), then the sedimentation rate would be 8×10^{-3} mm yr^{-1}, which is approximately 1-2 orders of magnitude lower than sedimentation rates recorded in northern Lake Malawi (Johnson et al., 2002), but approximately equal to our minimum estimate of the throw rate of the fault ($5 – 10 \times 10^{-3}$ mm yr^{-1},-assuming the footwall topography we have measured is an estimate of the minimum fault throw). Although this leaves open the possibility that some faults in the centre of the rift may have been buried by sedimentation, the lack of any more fault-related geomorphology along the River Shire (other than that seen in Figure 9), suggests we have not missed any major faults. Moreover, combining size-frequency and displacement-length fault scaling relations indicates that with a maximum fault length of ~50 km and a lower fault length of ~10 km we will have accounted for ~90 % of the tectonic strain in the region (Scholz and Cowie, 1990).

6.2. Age of the fault scarps

The faults in the Zomba Graben have offset the sedimentary cover, which includes coarse-grained sandstones of the Matope beds, as well as sandy, pebbly, fluvio-lacustrine deposits in the centre of the rift (Figure 2). However, the ages of these sediments have not been verivied by geochronological dating. Dulanya (2017) correlated the Matope beds with the Plio-Pleistocene development of the graben (the 'lower Upper Shire section' in Dulanya, 2017) based on stratigraphic mapping and age estimates from Bloomfield (1965). Optically-Stimulated Luminescence (OSL) ages for surficial palaeo-fluvio-lacustrine deposits near Lake Chilwa, 20-30 km to the east of the Zomba Graben, are <50 ka (Thomas et al., 2009; Figure 1).

The floor of the Zomba Graben, which is covered by both fine-grained fluvio-lacustrine sediments, and the coarse-grained Matope beds, lies ~10 m above the current level of lake Malawi. Since the Mid-Pleistocene Transition (MPT; ~800 ka), the level of Lake Malawi has fluctuated with high-stands up to ~150 m higher than the present lake level and low-stands up to ~500 m lower (Lyons, 2015; McCartney and Scholz, 2016; Owen et al, 1990). Although the exact magnitudes of these high- and low-stands are difficult to constrain, the last high-stand is thought to have begun at ~75 ka and continued to the present day (Ivory et al., 2016). Consequently, during high-stands, lacustrine conditions presumably flooded the Zomba graben, whereas low-stands were accompanied by the deposition of coarse-grained sediments (Lyons et al., 2011; 2015). Therefore, the fine- and coarse-grained sediments on the floor of the Zomba graben were likely deposited during the late-Quaternary, which implies that the fault scarps we observe that have offset and been draped by these sediments have formed during the late Quaternary time period: <800 ka and maybe as recently as <75-50 ka. A number of observations suggest that this interpretation is reasonable: i) The fault scarps are generally steep (Figure 3b & Figure 4a); and ii) fieldwork along the Mlungusi fault found the fault draped by a layer of sub-rounded to rounded cobbles (3-6 cm) in a clast-supported sandy matrix that is consistent with a lacustrine palaeobeach deposit, likely deposited during a high-stand within Lake Malawi during the late Quaternary (since the MPT ~800 ka). The heights of the measured scarps are generally greater than the displacements seen in single events for normal faults (e.g. Leonard, 2010), therefore the scarps should be viewed as composite scarps representing the cumulative offset from multiple earthquakes.

7. Strain Migration and Fault Evolution during rifting

Current conceptual models suggest that the transition from rift border faults to intrarift deformation occurs over timescales of 10-15 Ma in the East African Rift as lithospheric thinning leads to asthenospheric upwelling and production of magmatic fluids (Ebinger, 2005; Ebinger and Scholz, 2012; Buck, 2004). However, both our study and seismic reflection profiles of Lake Malawi (McCartney and Scholz, 2016) show that both border faults and intrabasin faults are active even in this amagmatic rift segment. The reflection studies have been unable to constrain the timing of the transition to axial deformation, but here we show that the proportion of strain accommodated in the interior of the Zomba Graben has increased from 25 ± 8% since the onset of rifting to 50 ± 25% over the since the fault scarps have been preserved in the late Quaternary (Figure 10). We discuss four mechanisms that may explain this changing strain pattern across a distributed network of faults in an apparently non-volcanic rift: 1) cessation of border fault activity; 2) lithospheric flexure; 3) a hidden fluid phase; and 4) transient changes associated with fault linkage. We then discuss whether the pattern of strain can be explained by the lithospheric structure, including crustal heterogeneities.

7.1. Cessation of Border Fault Activity and Lithospheric Flexure

The maximum amount of displacement a normal fault can accumulate, before it becomes more favourable to form a new fault, is thought to be controlled by a combination of effective elastic thickness, seismogenic thickness, and surface processes, such as footwall erosion and hanging wall deposition (Scholz and Contreras, 1998; Olive et al., 2014). The exact mechanism of fault abandonment is debated but it generally requires large total displacements (>5 km) that lead to an increase in the flexural restoring force and/or rotation of the fault dip to unfavourable angles (Scholz and Contreras, 1998; Goldsworthy and Jackson, 2001).

When rift border faults are abandoned, migration of fault activity into the hanging wall of the previously active fault is widely observed (see Goldsworthy and Jackson, 2001, for further discussion). Accardo et al. (2018) propose that the ~6 km of throw on the border faults in the northern and central basins of Lake Malawi indicates that these faults are approaching their maximum size and that the migration of strain into the rift interior is imminent or now occurring (e.g. the Karonga earthquake sequence; Biggs et al., 2010; Kolawole et al., 2018). However, this mechanism is unlikely to cause the late-Quaternary intrarift faulting in the Zomba Graben, because both the border and intrarift faults have been active during the late-Quaternary and the topographic relief is relatively small (<1 km). Similarly, bending forces associated with flexure of the border fault hanging wall can induce strain in the intrarift region within the upper crust, and although this has been proposed for Lake Malawi (Kolawole et al., 2018), the low throws and thick elastic crust (~30 km) in the Zomba Graben would generate negligible flexural strain (Jackson and Blenkinsop 1997, Muirhead et al 2016).

7.2. Influence of fluids

Magma-assisted rifting, where magmatic fluids and volatiles enable extension at lower stresses than the available tectonic forces, is thought to play an important role in facilitating rifting in thick continental lithosphere (Buck, 2004; Ebinger et al., 2017). There is no evidence of active magmatic activity or more than a few kilometres of crustal thinning in the Zomba Graben (Reed et al., 2016, Wang et al 2019). Furthermore, the geochemistry of hot springs in southern Malawi does not suggest a magmatic influence (Dulanya et al., 2010) and the nearest active volcano, Rungwe, is located ~700 km to the north (Figure 1). However, decompression melting or lower crustal magmatic intrusion might not lead to perceptible surface effects, and there is evidence for non-zero crustal thinning beneath southern Malawi (Wang et al., 2019). In an example further south and west in the EARS, low seismic velocities suggest decompression melting in the upper asthenosphere of the Okavango Delta, despite a very low level of extension and no surface volcanism or evidence for mantle upwelling (Yu et al., 2017).

Earthquakes occur in Malawi throughout the 38-42 km thick crust (Tedla et al., 2011; Jackson and Blenkinsop, 1993; Craig et al., 2011), consistent with estimates of effective elastic thickness in excess of 30 km (Ebinger et al., 1999). This can occur in magmatic rift zones if border faults penetrate into the lower crust, or if melt and volatile migration into the lower crust causes localised weakening, which can also trigger seismicity (Ebinger et al., 2017). However, current imaging of the lower crust in Malawi does not allow us to discriminate between these mechanisms and alternative explanations for the deep seismicity, that include 1) a dry, strong, granulite facies lower crust (Jackson et al., 2004), 2) above average lithospheric thickness (Chen and Molnar, 1983), or 3) localised zones of weak rheology within a strong, elastic lower crust (Fagereng, 2013).

7.3. Transient Changes Associated with Fault Evolution

The process of fault segment linkage can lead to an increase in fault slip rates over timescales of ~100 ka (Taylor et al., 2004). This can subsequently enable a newly linked fault to accommodate a greater proportion of the regional extension rate (Taylor et al., 2004; Cowie et al., 2005). We infer segment linkage on the Chingale Step fault that may have occurred as recently as the late-Quaternary (Figure 7), suggesting that faults in this region grow through linkage that occurs before they have accumulated significant (i.e. >1 km) offsets and on short timescales of < 800 ka (and possibly <~50 ka). This rapid linkage, before continued slip accumulation, is consistent with the recent hybrid fault growth model where slip accumulates at a constant fault length after an initial growth phase (Rotevatn et al., *in press*). The segment linkage we observe may have driven the apparent increase in strain within the rift interior. However, when faults are closely spaced, as they are in the Zomba Graben, across-strike co-seismic elastic stress changes can also drive transient variations in fault slip rates (Cowie et al., 2012). Elastic interactions between faults can therefore change slip rates on individual faults over the time scale of a few earthquake cycles (Cowie et al., 2012). With only one example, we cannot tell whether the observed increase in intra-rift strain is a long-lived feature of the rift, or a transient feature only representative of the time window we sampled (i.e. since the fault scarps have been preserved in the late-Quaternary). Nonetheless, although elastic fault interactions are likely contributing to the temporal evolution of strain across the network of faults in the Zomba Graben, they cannot explain the initial formation of a distributed fault network.

7.4. Lithospheric Structure

The roles of crustal thickness, lower crustal rheology, and lithospheric thermal structure in developing end-member narrow or wide rifts have been well studied (e.g. Buck, 1991;

Huismans and Beaumont, 2007). Typically, strain in narrow rifts concentrates in the weakest part of the lithosphere while in wide rifts, lower crustal viscous flow drives distributed deformation in the upper crust (Buck, 1991). Southern Africa has unusually thick continental lithosphere (140-180 km; Craig et al., 2011), resulting from multiple episodes of orogenic thickening (Fritz et al., 2013), and 38-42 km thick crust (Tedla et al., 2011, Wang et al 2019). The available constraints on the lithospheric properties of the Zomba Graben suggest that conditions are similar to the very young (120-40 Ka) Okavango Rift (Craig et al., 2011). However, we have demonstrated that strain within the narrow (<50 km) Zomba Graben is distributed whereas the Okavango Rift is >150 km wide and deformation is localised to <50 km wide zones at the edges of the rift (Ebinger and Scholz, 2012). Thus, the currently-available constraints on lithospheric properties cannot explain the differences between these two rifts.

Numerical simulations demonstrate that a strong, ductile lower crust promotes distributed faulting due to enhanced upper crustal fault interactions during rifting (Heimpel and Olson, 1996). The crust in southern Malawi is made up of high grade metamorphic fabrics that lack hydrous minerals with low friction coefficients (Hellebrekers, et al. *in review*), and exposed fault rocks are not demonstrably different in composition from these high grade basement rocks (Williams et al., *submitted.*). Thus, distributed faulting in the Zomba Graben cannot be attributed to reactivation of pre-existing frictionally weak planes in the brittle regime. However, lateral heterogeneity in the lower crust, such as an anastomosing shear zone system, would enable strain localisation in lower viscosity zones in an otherwise cold, strong layer (Fagereng, 2013). Such localisation at depth may guide deformation patterns in the overlying brittle crust, such as the oblique strike of faults in southern Malawi, relative to the regional extension direction (Hodge et al., 2018; Williams et al., *in review*).

The hypothesis of a lower crust with rheological heterogeneity: i) satisfies the requirements for a dominantly strong lower crust; ii) can explain the deep seismicity observed in the Malawi rift; iii) facilitates the formation of a distributed fault network at the surface; and iv) does not require pre-existing frictional weaknesses in the upper crust. This suggests that patterns of strain distribution in amagmatic rifts may not be solely controlled by rift maturity; instead, rheological heterogeneity in the lower crust and elastic fault interactions in the upper crust may also have important effects.

8. Implications for Seismic Hazard.

Our analysis of high-resolution satellite topography has identified five active faults in the Zomba Graben, but current assessments of seismic hazard in Malawi do not extend south of Lake Malawi (Midzi et al., 1999; Hodge et al., 2015). Based on standard scaling laws (Leonard, 2010), these 15-50 km long faults could host earthquakes of Mw 6.3-7.1, assuming that faults do not fail in smaller individual segments, and that multiple separate faults do not slip in the same event. The administrative regions within 30 km of the Zomba Graben contains ~22% of the Malawian population (~ 4 million people), including the major population and administrative centres of Blantyre (population: ~800,000) and Zomba (population: ~100,000; Malawi National Statistics Office, 2018). The proximity of these newly-identified faults to this number of people presents a significant challenge for both seismic risk and regional development. Furthermore, the path of the Shire River is strongly affected by rift topography, and a large earthquake on the Mlungusi fault in particular could affect both irrigation and flooding on a regional scale as well as dam stability on the Shire

River. This is particularly important as ~80% of Malawi's electricity is generated by hydroelectric dams within the middle Shire valley (Taulo et al., 2015).

In slowly deforming regions and/or regions with poor seismic detection infrastructure, even decadal long instrumental catalogues are unlikely to record a representative enough sample of seismicity to sufficiently assess seismic hazard. Including fault maps in probabilistic seismic hazard analysis can overcome this problem (Pace et al., 2018), but this requires estimates of both earthquake magnitude and recurrence interval. In Lake Malawi, where fault slip rates have not been measured, Hodge et al. (2015) assigned the plate motion to individual faults in their hazard assessment. However, the discovery of multiple, subparallel fault scarps in the Zomba Graben suggests longer earthquake recurrence times and lower probabilities of peak ground acceleration for a given return period. Furthermore, increases in the number of faults within a region also leads to more variable fault slip rates, which in turn can result in earthquake clusters (Cowie et al., 2012). The 2009 Karonga earthquake sequence in northern Malawi illustrates that such clusters occur in the East African Rift (Biggs et al., 2010), but instrumental records are not sufficient to determine how widespread this behaviour is. Earthquake clusters present an additional challenge for seismic hazard assessment as they are not captured by time-independent probabilistic seismic hazard assessments.

9. Conclusion

We analyse high-resolution TanDEM-X data to identify late-Quaternary faults scarps on five faults in the Zomba Graben, southern Malawi. We compared the activity of the faults in the graben since the onset of rifting with the displacement accumulated since fault scarps have been preserved at the base of footwall escarpments. We show how 75 ± 18 % of strain was distributed on the border faults since the onset of rifting whereas in the more recent past, since the active fault scarps have been formed, ~50% of the strain has accumulated within the rift interior. This presents new insights into the behaviour of rifts during the incipient stages of continental extension in a region of thick lithosphere and no active volcanism. In contrast to the prevailing paradigm, it suggests that early, amagmatic stages of continental extension can be distributed across both rift border and intra-rift faults. We find evidence for linkage of fault segments within the rift interior that occurs prior to the accumulation of significant fault offset, and possibly on rapid, late-Quaternary timescales. While the overall mode of rifting is likely to be controlled by the rheology of the lithosphere, we suggest that upper-crustal fault interactions and strength variations within the lower crust can lead to spatially distributed and temporally transient faulting within early stage rifts. Finally, we find that the onshore rift in Southern Malawi represents a significant, but previously unappreciated source of seismic hazard within the East African Rift.

10. Acknowledgements

This work was funded by the EPSRC project 'Prepare' (EP/P028233/1), funded under the Global Challenges Research Fund. We thank Kondwani Dombola for his assistance with fieldwork planning and logistics. TanDEM-X data were obtained via DLR proposal DEM_GEOL0686

11. References

Accardo, N. J., Shillington, D. J., Gaherty, J. B., Scholz, C. A., Nyblade, A. A., Chindandali, P. R. N. et al. (2018). Constraints on Rift Basin Structure and Border Fault Growth in the Northern Malawi Rift From 3-D Seismic Refraction Imaging. *Journal of Geophysical Research: Solid Earth*. https://doi.org/10.1029/2018JB016504

Avouac, J-P. (1993). Analysis of scarp profiles: Evaluation of errors in morphological dating. *Journal of Geophysical Research: Solid Earth*, 98(B4), 6745-6754. https://doi.org.10.1029/92JB01962

Biggs, J., Nissen, E., Craig, T., Jackson, J., & Robinson, D. P. (2010). Breaking up the hanging wall of a rift-border fault: The 2009 Karonga earthquakes, Malawi. *Geophysical Research Letters*, 37, L11305. https://doi.org/10.1029/2010GL043179

Bloomfield, K. (1965). The Geology of the Zomba Area. *Bulletin of the Geological Survey Department, Malawi*, 16, 223p.

Bloomfield, K., & Garson, M. S. (1965). The Geology of the Kirk Range-Lisungwe Valley Area. *Bulletin of the Geological Survey Department, Malawi*, 17, 239p

Boulton, S. J., & Whittaker, A. C. (2009). Quantifying the slip rates, spatial distribution and evolution of active normal faults from geomorphic analysis: Field examples from an oblique-extensional graben, southern Turkey. *Geomorphology*, 104, 299-316. https://doi.org/10.1016/j.geomorph.2008.09.007

Buck, W. R. (1991). Modes of continental lithospheric extension. *Journal of Geophysical Research: Solid Earth*, 96(B12), 20161-20178. https://doi.org/10.0129/91JB01485

Buck, W. R. (2004). Consequences of asthenospheric variability on continental rifting. In G. D. Karner, N. W. Driscoll, B. Taylor, D. L. Kohlstedt (Eds), *Rheology and Deformation of the Lithosphere at Continental Margins* (pp. 1-30). New York: Columbia University Press.

Calais, E., Ebinger, C., Hartnady, C., & Nocquet, J. M. (2006). Kinematics of the East African Rift from GPS and earthquake slip vector data. *Geological Society, London, Special Publications*, 259, 9-22. https://doi.org/10.1144/GSL.SP.2006.259.01.03

Chen, W.-P., & Molnar, P. (1983). Focal depths of intracontinental and intraplate earthquakes and their implications for the thermal and mechanical properties of the lithosphere. *Journal of Geophysical Research: Solid Earth*, 88(B5), 4183-4214. https://doi.org/10.1029/JB088iB05p04183

Chorowicz, J., & Sorlien, C. (1992). Oblique extensional tectonics in the Malawi Rift, Africa. *GSA Bulletin*, 104(8), 1015-1023. https://doi.org/10.1130/0016-7606(1992)104<1015:OETITM>2.3.CO;2

Collettini, C., Sibson, R. H. (2001). Normal faults, normal friction? *Geology*, 29(10), 927-930. https://doi.org/10.1130/0091-7613(2001)029<0927:NFNF>2.0.CO;2

Contreras, J., Anders, M. H., & Scholz, C. H. (2000). Growth of a normal fault system: observations from the Lake Malawi basin of the east African rift. *Journal of Structural Geology*, 22(2), 159-168. https://doi.org/10.1016/S0191-8141(99)00157-1

Copley, A., Hollingsworth, J., & Bergman, E. (2012). Constraints on fault and lithosphere rheology from the coseismic slip and postseismic afterslip of the 2006 Mw7.0 Mozambique earthquake. *Journal of Geophysical Research: Solid Earth*, 117, B03404. https://doi.org/10.1029/2011JB008580

Cowie, P. A., Roberts, G. P., Bull, J. M. & Visini, F. (2012). Relationships between fault geometry, slip rate variability and earthquake recurrence in extensional settings. *Geophysical Journal International*, 189(1), 143-160. https://doi.org/10.1111/j.1365-246X.2012.05378.x

Cowie, P. A., Underhill, J. R., Behn, M. D., Lin, J., & Gill, C. (2005). Spatio-temporal evolution of strain accumulation derived from multi-scale observations of Late Jurasic rifting in the northern North Sea: A critical test of models of lithospheric extension. *Earth and Planetary Science Letters*, 234, 401-419. https://doi.org/10.1016/j.epsl.2005.01.039

Craig, T. J., Jackson, J. A., Priestley, K., & McKenzie, D. (2011). Earthquake distribution patterns in Africa: their relationship to variations in lithospheric and geological structure, and their rheological implications. *Geophysical Journal International*, 185(1), 403-434. https://doi.org/10.1111/j.1365-246X.2011.04950.x

Delvaux, D., & Barth, A. (2010). African stress pattern from formal inversion of focal mechanism data. *Tectonophysics*, 482, 105-128. https://doi.org/10.1016/j.tecto.2009.05.009

Dixey, F. (1926). The Nyasaland Section of the Great Rift Valley. *The Geographical Journal*, 68(2), 117-137.

Dixey, F. (1938). The Nyasa-Shire Rift. *The Geographical Journal*, 91(1), 51-56. doi:10.2308/1787817

Dulanya, Z. (2017). A review of the geomorphotectonic evolution of the south Malawi rift. *Journal of African Earth Sciences*, 129, 728-738. http://dx.doi.org/10.1016/j.jafrearsci.2017.02.016

Dulanya, Z., Norales-Simfors, N., & Sivertun, Å. (2010). Comparative study of the silica and cation geothermometry of the Malawi hot springs: Potential alternative energy source. *Journal of African Earth Sciences*, 57(4) 321-327. https://doi.org/10.1016/j.afrearsci.2009.11.001

Ebinger, C. J. (2005). Continental break-up: The East African perspective. *Astronomy & Geophysics*, 46(2), 16-21. https://doi.org/10.1111/j.1468-4004.2005.46216.x

Ebinger, C. J., Deino, A. L., Tesha, A. L., Becker, T., & Ring, U. (1993). Tectonic controls on rift basin morphology: Evolution of northern Malawi (Nyasa) Rift, *Journal of Geophysical Research: Solid Earth*, 98(B10), 17821-17836. https://doi.org/10.1029/93JB01392

Ebinger, C. J., Jackson, J. A., Foster, A. N., & Hayward, N. J. (1999). Extensional basin geometry and the elastic lithosphere. *Philosophical Transactions of the Royal Society A*, 357(1753), 741-765. https://doi.org/10.1098/rsta.1999.0351

Ebinger, C. J., Keir, D., Bastow, I. D., Whaler, K., Hammond, J. O. S., Ayele, A., Miller, M. S., Tiberi, C., & Hautot, S. (2017). Crustal structure of active deformation zones in Africa: implications for global crustal processes. *Tectonics*, 36, 3298-3332. https://doi.org/10.1002/2017TC004526

Ebinger, C. J., Rosendahl, B. R., & Reynolds, D. J. (1987). Tectonic model of the Malawi rift, Africa. *Tectonophysics*, 141(1-3), 215-235. https://doi.org/10.1016/0040-1951(87)90187-9

Ebinger, C. J., & Scholz, C. A. (2012). Continental rift basins: the East African perspective. In C. Busby, A. Azor (Eds), *Tectonics of Sedimentary Basins: Recent Advances* (pp. 185-208). Chichester, UK: John Wiley & Sons.

Eby, G. N., Roden-Tice, M., Krueger, H. L., Ewing, W., Faxon, E. H., & Woolley, A. R. (1995). Geochronology and cooling history of the northern part of the Chilwa Alkaline Province, Malawi. *Journal of African Earth Sciences*, 20(3-4), 275-288. https://doi.org/10.1016/0899-5362(95)00054-W

England, P., & Molnar, P. (1997). The field of crustal velocity in Asia calculated from Quaternary rates of slip on faults. *Geophysical Journal International*. 130(3), 551-582. https://doi.org/10.1111/j.1365-246X.1997.tb01853.x

Fagereng, Å. (2013). Fault segmentation, deep rift earthquakes and crustal rheology: Insights from the 2009 Karonga sequence and seismicity in the Rukwa-Malawi rift zone. *Tectonophyisics*, 601, 216-225. https://doi.org/10/1016/j.tecto.2013.05.012

Flannery, J. W., & Rosendahl, B. R. (1990). The seismic stratigraphy of Lake Malawi, Africa: implications for interpreting geological processes in lacustrine rifts. *Journal of African Earth Sciences (and the Middle East)*, 10(3), 519-548. https://doi.org/10.1016/0899-5362(90)90104-M

Fritz, H., Abdelsalam, M., Ali, K. A., Bingen, B., Collins, A. S., Fowler, A. R., et al. (2013). Orogen styles in the East African Orogen: A review of the Neoproterozoic to Cambrian tectonic evolution. *Journal of African Earth Sciences*. 86, 65-106. https://doi.org/10.1016/j.afrearsci.2013.06.004.

Goldsworthy, M. & Jackson, J. (2001). Migration of activity with normal fault systems: examples from the Quaternary of mainland Greece. *Journal of Structural Geology*, 23(2-3), 489-506. https://doi.org/10.1016/S0191-8141(00)00121-8

Heimpel, M., & Olson, P. (1996). A seismodynamical model of lithosphere deformation: Development of continental and oceanic rift networks. *Journal of Geophysical Research: Solid Earth*, 101(B7). https://doi.org/10.1029/96JB00168

Hellebrekers, N., Niemeijer, A. R., Fagereng, Å., Manda, B., & Mvula, R. L. S. Lower crustal earthquakes in the East African Rift System: Insights from frictional properties of rock samples from the Malawi rift. *In review with Tectonophyiscs*.

Hodge, M., Biggs, J., Goda, K., & Aspinall, W. (2015). Assessing infrequent large earthquakes using geomorphology and geodesy: the Malawi Rift. *Natural Hazards*, 76, 1781-1806. https://doi.org/10.1007/s11069-014-1572-y

Hodge, M., Biggs, J., Fagereng, Å., Elliot, A., Mdala, H., Mphepo, F. (2019). A semi-automated algorithm to quantify scarp morphology (SPARTA): application to normal faults in southern Malawi. *Solid Earth*, 10, 27-57. https://doi.org/10.5194/se-10-27-2019

Hodge, M., Fagereng, Å., Biggs, J., & Mdala, H. (2018). Controls on Early-Rift Geometry: New Perspectives From the Bilila-Mtakataka Fault, Malawi. *Geophysical Research Letters*, 45. https://doi.org/10.1029/2018GL077343

Huismans, R. S., & Beaumont, C. (2007). Roles of lithospheric strain softening and heterogeneity in determining the geometry of rifts and continental margins. In G. D. Karner, G. Manatschal, L. M. Pihheiro (Eds), *Imaging, Mapping and Modelling Continental Lithosphere Extension and Breakup* (pp. 111-138). London, UK: Geological Society, London, Special Publications.

Ivory, S. J., Blome, M. W., Kking, J. W., McGlue, M. M., Cole, J. E., & Cohen , A. S. (2016). Environmental change explains cichlid adaptive radiation at Lake Malawi over the past 1.2 million years. *Proceedings of the National Academy of Sciences of the United States of America*, 113(42), 11895-11900. https://doi.org/10.1073/pnas.1611028113

Jackson, J. A., Austrheim, H., McKenzie, D., & Priestley, K. (2004). Metastability, mechanical strength, and the support of mountain belts. *Geology*, 32(7), 625-628. https://doi.org/10.1130/G20397.1

Jackson, J., & Blenkinsop, T. (1993). The Malawi Earthquake of March 10, 1989: Deep faulting with the East African Rift System. *Tectonics*, 12(5), 1131-1139. https://doi.org/10.1029/93TC01064

Kolawole, F., Atekwana, E. A., Laó-Dávila, D. A., Abdelsalam, M. G., Chindandali, P. R., Salima, J., & Kalindekafe, L. (2018b). Active Deformation of Malawi Rift's North Hinge Zone Modulated by Reactiviation of Preexisting Precambrian Shear Zone Fabric. *Tectonics*, 37, 683-704. https://doi.org/10.1002/2017TC004628

Kostrov, V. V. (1974). Seismic moment and energy of earthquakes, and seismic flow of rock. *Physics of the Solid Earth*, 1, 13-21.

Laó-Dávila, D. A., Al-Salmi, H. S., Abdelsalam, M. G., & Atekwana, E. A. (2015). Hierarchical segmentation of the Malawi Rift: The influence of inherited lithospheric heterogeneity and kinematics in the evolution of continental rifts. *Tectonics*, 34, 2399-2417. https://doi.org/10.1002/2015TC003953

Leonard, M. (2010). Earthquake Fault Scaling: Self-Consistent Relating of Rupture Length, Width, Average Displacement, and Moment Release. *Bulletin of the Seismological Society of America*, 100(5a), 1971-1988. https://doi.org/10.1785/0120090189

Lloyd, R., Biggs, J., & Copley, A. (*in press)*. The decade-long Machaze-Zinave aftershock sequence in the slowly straining Mozambique Rift. *Geophysical Journal International*. https://doi.org/10.1093/gji/ggz033

Lyons, R. P., Scholz, C. A., Buoniconti, M. R., & Martin, M. R. (2011). Late Quaternary stratigraphic analysis of the Lake Malawi Rift, East Africa: An integration of drill-core and seismic-reflection data. *Palaeogeography, Palaeoclimatology, Palaeoecology*, 303(1-4), 20-37, https://doi.org/10.1016/j.palaeo.2009.04.014

Lyons, R. P., Scholz, C. A., Buoniconti, M. R., & Martin, M. R. (2011). Late Quaternary stratigraphic analysis of the Lake Malawi Rift, East Africa: An integration of drill-core and seismic-reflection data. *Palaeogeography, Palaeoclimatology, Palaeoecology*, 303(1-4), 20-37, https://doi.org/10.1016/j.palaeo.2009.04.014

McCartney, T., & Scholz, C. A. (2016). A 1.3 million year record of synchronous faulting in the hangingwall and border fault of a half-graben in the Malawi (Nyasa) Rift. *Journal of Structural Geology*, 91, 114-129. http://dx.doi.org/10.1016/j.jsg.2016.08.012

Malawi National Statistics Office, (2018). 2018 Malawi Population & Housing Census: Preliminary Report. Government of Malawi. 55pp.

Midzi, V., Hlatywayo, D. J., Chapola, L. S., Kebede, F., Atakan, K., Lombe, D. K., Turyomurugyendo, G., & Tugume, F. A. (1999). Seismic hazard assessment in Eastern and Southern Africa. *Annals of Geophysics*, 42(6), 1067-1083. https://doi.org/10.4401/ag-3770

Montgomery, D. R., & Brandon, M. T. (2002). Topographic controls on erosion rates in tectonically active mountain ranges. *Earth and Planetary Science Letters*, 201(3-4), 481-489. https://doi.org/10/1016/S0012-821X(02)00725-2

Mortimer, E., Kirstein, L., Stuart, F. M., & Strecker, M. R. (2016a). Spatio-temporal trends in normal-fault segmentation recorded by low-temperature thermochronology: Livingstone fault scarp, Malawi Rift, East African Rift System. *Earth and Planetary Science Letters*, 455, 62-72. http://dx.doi.org/10.1016/j.epsl.2016.08.040

Muirhead, J. D., Kattenhorn, S. A., Lee, H., Mana, S., Turrin, B. D., Fischer, T. P. et al. (2016). Evolution of upper crustal faulting assisted by magmatic volatile during early-stage continental rift development in the East African Rift. *Geosphere*, 12(6), 1670-1700. https://doi.org/10.1130/GES01375.1

Muirhead, J. D., Wright, L. J. M., & Scholz, C. A. (2019). Rift Evolution in regions of low magma input in East Africa. *Earth and Planetary Science Letters*, 506, 332-346. https://doi.org/10.1016/j.epsl.2018.11.004

Olive, J-A., Behn, M. D., & Malatesta, L. C. (2014). Modes of extensional faulting controlled by surface processes. *Geophysical Research Letters*, 41(19), https://doi.org/10.1002/2014GL061507

Owen, R. B., Crossley, R. Johnson, T. C., Tweddle, D., Kornfield, I., Davison, S., Eccles, D. H., & Engstrom, D. E. (1990). Major low levels of Lake Malawi and their implications for speciation rates in cichlid fishes. *Proceedings of the Royal Society B*, 240 (1299), 519-553. https://doi.org/10.1098/rspb.1990.0052

Pace, B., Visini, F., Scotti, O., & Peruzza, L. (2018). Preface: Linking faults to seismic hazard assessment in Europe. *Natural Hazards and Earth Systems Sciences*, 18, 1349-1350. https://doi.org/10.5194/nhess-18-1349-2018

Rotevatn, A., Jackson, C. A. L., Tvedt, A. B., Bell, R. E., & Blækkan, I. (*in press*). How do normal faults grow? *Journal of Structural Geology*, https://doi.org/10.1016.j.jsg.2018.08.005

Reed, C. A., Liu, K. H., Chindandali, P. R. N., Massingue, B., Mdala, H., Muamina, D., Yu, Y., & Gao, S. S. (2016). Passive rifting of thick lithosphere in the southern East African Rift: Evidence from mantle transition zone discontinuity topography. *Journal of Geophysical Research: Solid Earth*. 121(11), https://doi.org/10.1002/2016JB013131

Roberts, E. M., Stevens, N. J., O'Connor, P. M., Dirks, P. H. G. M., Gottfied, M. D., Clyde, W. C. et al. (2012). Initiation of the western branch of the East African Rift coeval with the eastern branch. *Nature Geoscience*, 5, 289-294. https://doi.org/10.1038/ngeo1432

Saria, E., Calais, E., Stamps, D. S., Delvaux, D., & Hartnady, C. J. H. (2014). Present-day kinematics of the East African Rift. *Journal of Geophysical Research: Solid Earth*, 119(4), 3584-3600. https://doi.org/10.1002/2013JB010901

Scholz, C. A. (1995). Deltas of Lake Malawi rift, east Africa: Seismic expression and exploration implications. *AAPG Bulletin*, 79 (11). https://doi.org/10.1306/7834DE54-1721-11D7-8645000102C1865D

Scholz, C. A., & Rosendahl, B. R. (1988). Low Lake Stands in Lakes Malawi and Tanganyika, East Africa, Delineated with Multifold Seismic Data. *Science*, 240, 1645-1648. https://doi.org/10.1126/science.240.4859.1645

Scholz, C. H., & Contreras, J. C. (1998). Mechanics of continental rift architecture. *Geology*, 26(11), 967-970. https://doi.org/10.1130/0091-7613(1998)026<0967:MOCRA>2.3.CO;2

Scholz, C. H., & Cowie, P. A. (1990). Determination of total strain from faulting using slip measurements. *Nature*, 346, 837-839.

Schwanghart, W., & Scherler, D. (2014). TopoTooolbox 2 – MATLAB-based software for topographic analysis and modelling in Earth surface sciences. *Earth Surface Dynamics*, 2, 1-7. https://doi.org/10.5194/esurf-2-1-2014

Shillington, D. J., Gaherty, J. B., Ebinger, C. J., Scholz, C. A., Selway, K., Nyblade, A. A. et al. (2016). Acquisition of a Unique Onshore/Offshore Geophysical and Geochemical Dataset in the Northern Malawi (Nyasa) Rift. *Seismological Research Letters*, 87(6), 1406-1416. https://doi.org/10.1785/0220160112

Specht, T. D., & Rosendahl, B. R. (1989). Architecture of the Lake Malawi Rift, East Africa. *Journal of African Earth Sciences (and the Middle East)*, 8(2-4), 355-382. https://doi.org/10.1016/S0899-5362(89)80032-6

Stamps, D. S., Saria, E., & Kreemer, C. (2018). A Geodetic Strain Rate Model for the East African Rift System. *Scientific Reports*, 8, 732. https://doi.org/10.1038/s41598-017-19097-w

Taulo, J. L., Gondwe, K. J., & Sebitosi, A. B. (2015). Energy supply in Malawi: Options and issues. *Journal of Energy in Southern Africa*, 26(2) 19-32.

Taylor, S. K., Bull, J. M., Lamarche, G. & Barnes, P. M. (2004). Normal fault growth and linkage in the Whakatane Graben, New Zealand, during the last 1.3 Myr. *Journal of Geophysical Research: Solid Earth*, 109(B2). https://doi.org/10.1029/2003JB002412

Tedla, G. E., van der Meijde, M., Nyblade, A. A., & van der Meer, F. D. (2011). A crustal thickness map of Africa derived from a global gravity field model using Euler deconvolution. *Geophysical Journal International*, 187(1), 1-9. https://doi.org/10.1111/j.1365-246X.2011.05140.x

Thomas, D. S. G., Bailey, R., Shaw, P. A., Durcan J. A., & Singarayer, J. S. (2009). Late Quaternary highstands at Lake Chilwa, Malawi: Frequency, timing and possible forcing mechanisms in the last 44 ka. *Quaternary Science Reviews*, 28, 526-539. https://doi.org/10.1016/jquascirev.2008.10.023

Wang, T., Feng, J., Liu, K. H., Gao, S. S. (2019). Crustal structure beneath the Malawi and Luangwa Rift Zones and adjacent areas from ambient noise tomography. *Gondwana Research*, 67, 187-198. https://doi.org/10.1016/j.gr.2018.10.018

Wernicke, B., & Axen, G. J. (1988). On the role of isostasy in the evolution of normal fault systems. *Geology*, 16(9), 848-851. https://doi.org/10.1130/0091-7613(1988)016<0848:OTROII>2.3.CO;2

Wessel, B., Huber, M., Wohlfart, C., Marschalk, U., Kosmann, D., Roth, A. (2018). Accuracy assessment of the global TanDEM-X Digital Elevation Model with GPS data. *ISPRS Journal of Photogrammetry and Remote Sensing*, 139, 171-182. https://doi.org/10.1016/j.isprsjprs.2018.02.017

Wessel, P. & Smith, W.H. (1998), New, improved version of Generic Mapping Tools released. *Eos, Transactions American Geophysical Union*, 79, 579.

Whipple, K. X., & Tucker, G. E. (1999). Dynamics of the stream-power river incision model: Implications for height limits of mountain ranges, landscape response timescales, and research needs. *Journal of Geophysical Research: Solid Earth*, 104(B8), 17661-17674. https://doi.org/10.1029/1999JB900120

Williams, J. N., Fagereng, Å., Wedmore, L. N. J., Biggs, J., Mphepo, F., Dulanya, Z., Mdala, H., & Blenkinsop, T. *In review with Geochemistry, Geophysics, Geosystems*.

Wobus, C., Whipple, K. X., Kirby, E., Snyder, N., Johnson, J., Spyropolou, K. et al. (2006). Tectonics from topography: Procedures, promise and pitfalls. In S. D. Willet, N. Hovius, M. T. Brandon, & D. M. Fisher (Eds). *Tectonics, Climate and Landscape Evolution*, (pp. 55-74). Geological Society of America: Special Paper 398. https://doi.org/10.1130/2006.2398(04)

Yu, Y., Liu, K. H., Huang, Z., Zhao, D., Reed, C. A., Moidaki, M., Lei, J., & Gao, S. S. (2017). Mantle structure beneath the incipient Okavango rift zone in southern Africa. *Geosphere*, 13(1), 102-111. https://doi.org/10.1130/GES01331.1

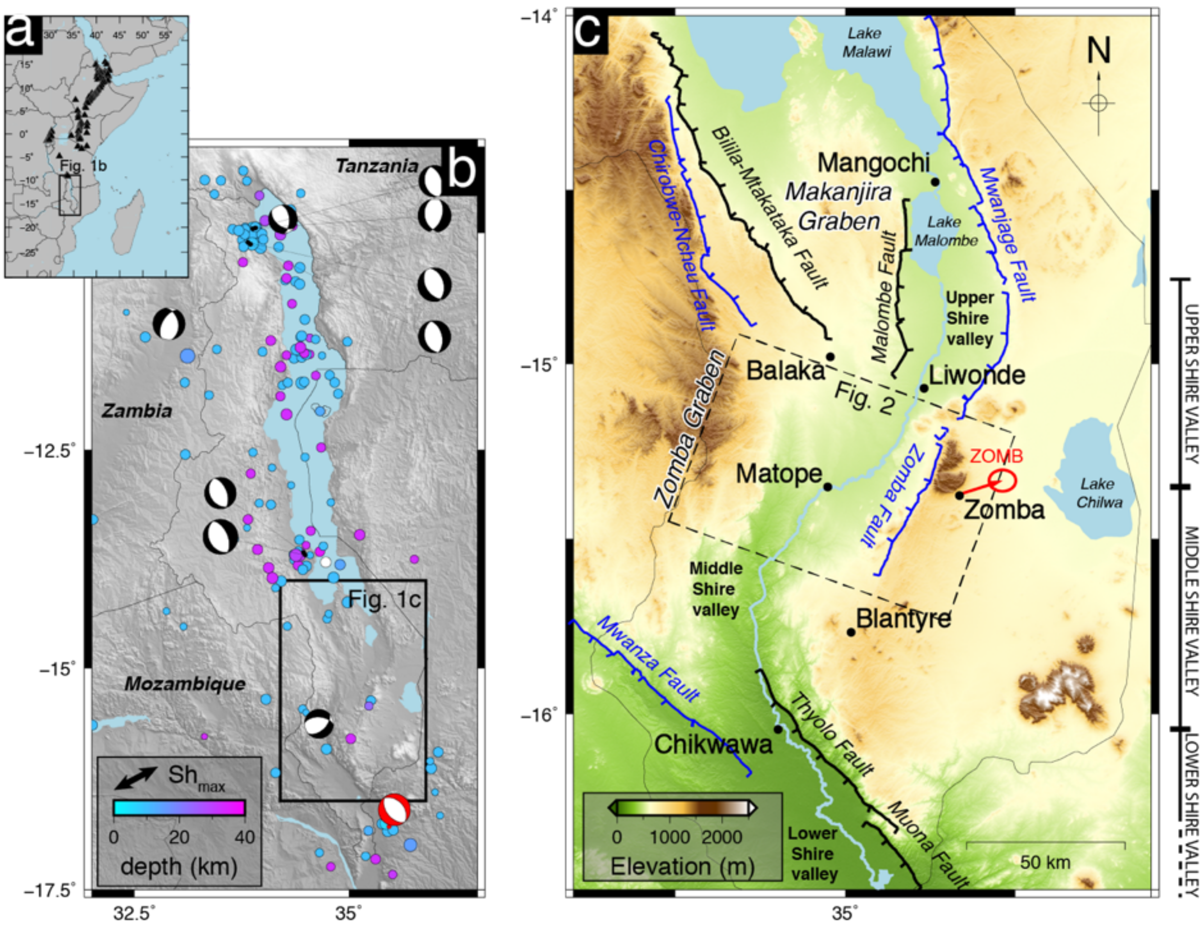

Figure 1: The location of the Zomba Graben within the East African Rift and Malawi. (a) The location of Malawi within the East African Rift. Black triangles show the active volcanoes within the rift. (b) Seismicity in the Malawi rift and the location of the Zomba Graben. Dots show National Earthquake Information Centre (NEIC) earthquakes from 1971-2018 coloured by depth. Focal mechanisms for all events greater than M_w5.0 are from Craig et al. (2010) with the exception of the red focal mechanism which shows the location and CMT mechanism of the 17th March 2018 Nsanje earthquake. The Sh_{max} direction is from Delvaux and Barth (2010). (c) Overview map of southern Malawi showing the location of the Zomba Graben relative to other known faults in the region. Faults where scarps have been detected and measured are indicated in black. Faults which are suspected as active but with no

measurements of throw or where no fault scarp has previously been detected are shown in blue. GPS vector from Stamps et al. (2018) is shown in red.

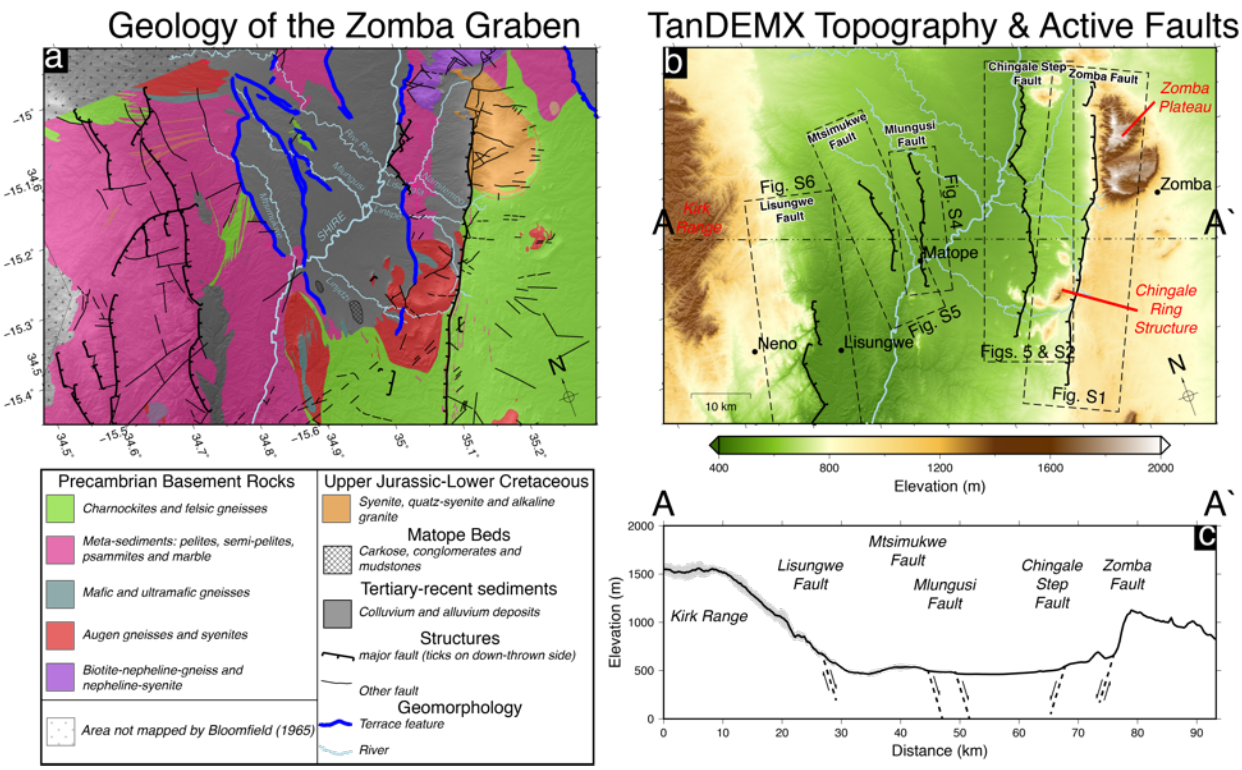

Figure 2: Geology and topography of the Zomba Graben. (a) Geological map of the Zomba Graben adapted from Bloomfield (1965). (b) TanDEMX digital elevation model of the Zomba Graben. (c) Swath topographic profile across the Zomba Graben. The gray shading indicates the maximum and minimum topography in a 5km either side of the dashed line in part b. The solid line indicates the mean elevation.

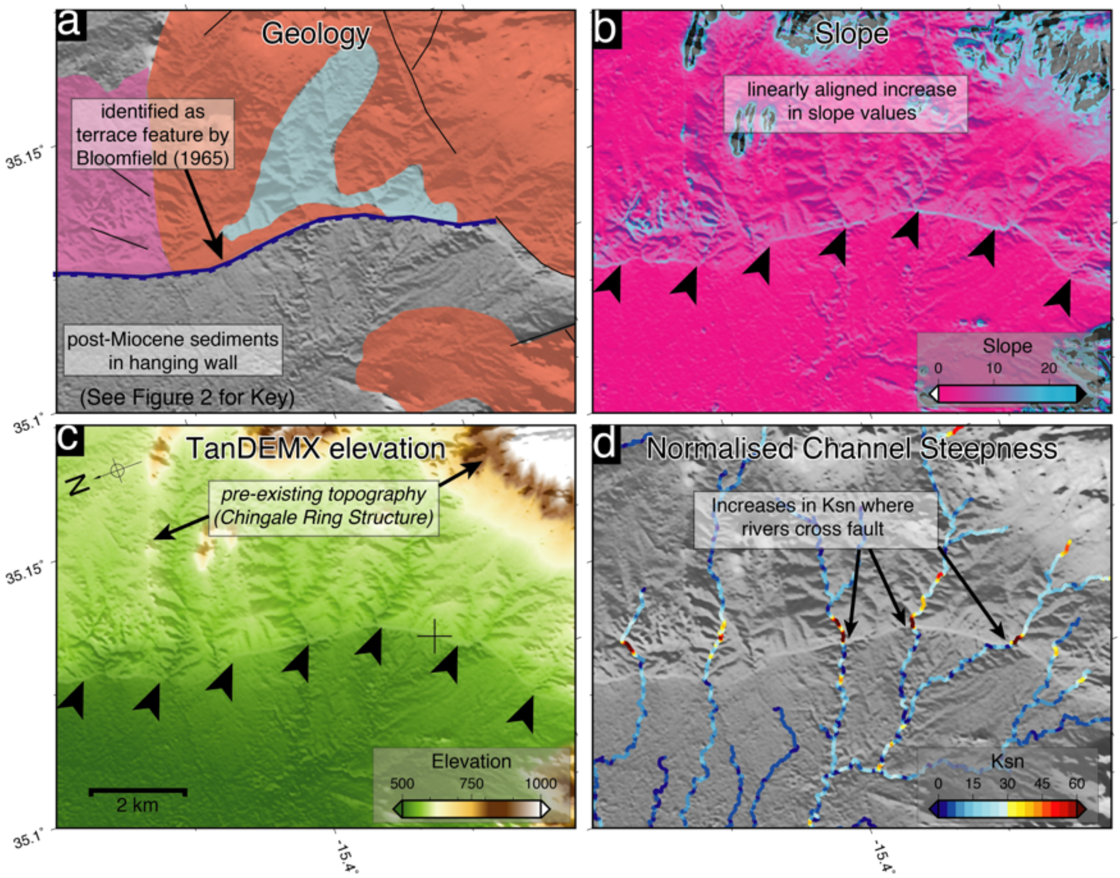

Figure 3: The method used to identify and measure the activity of the faults in the Zomba Graben. A small section of the Chingale fault is used as an example. For full details of each fault see the supplementary material. (a) Geological maps (Bloomfield, 1965) were used to identify locations where scarps or terrace features had Tertiary-recent sediments in their hangingwall. (b) TanDEMX DEM, with the location of the fault identified by the change in elevation and indicated by the black arrows. (c) Slope map that shows a linearly aligned increase in slope values that correspond to the terrace feature in part a and the increase in topography in part b. (d) The normalised channel steepness index increases in the footwall of the fault as the river channels cross the fault.

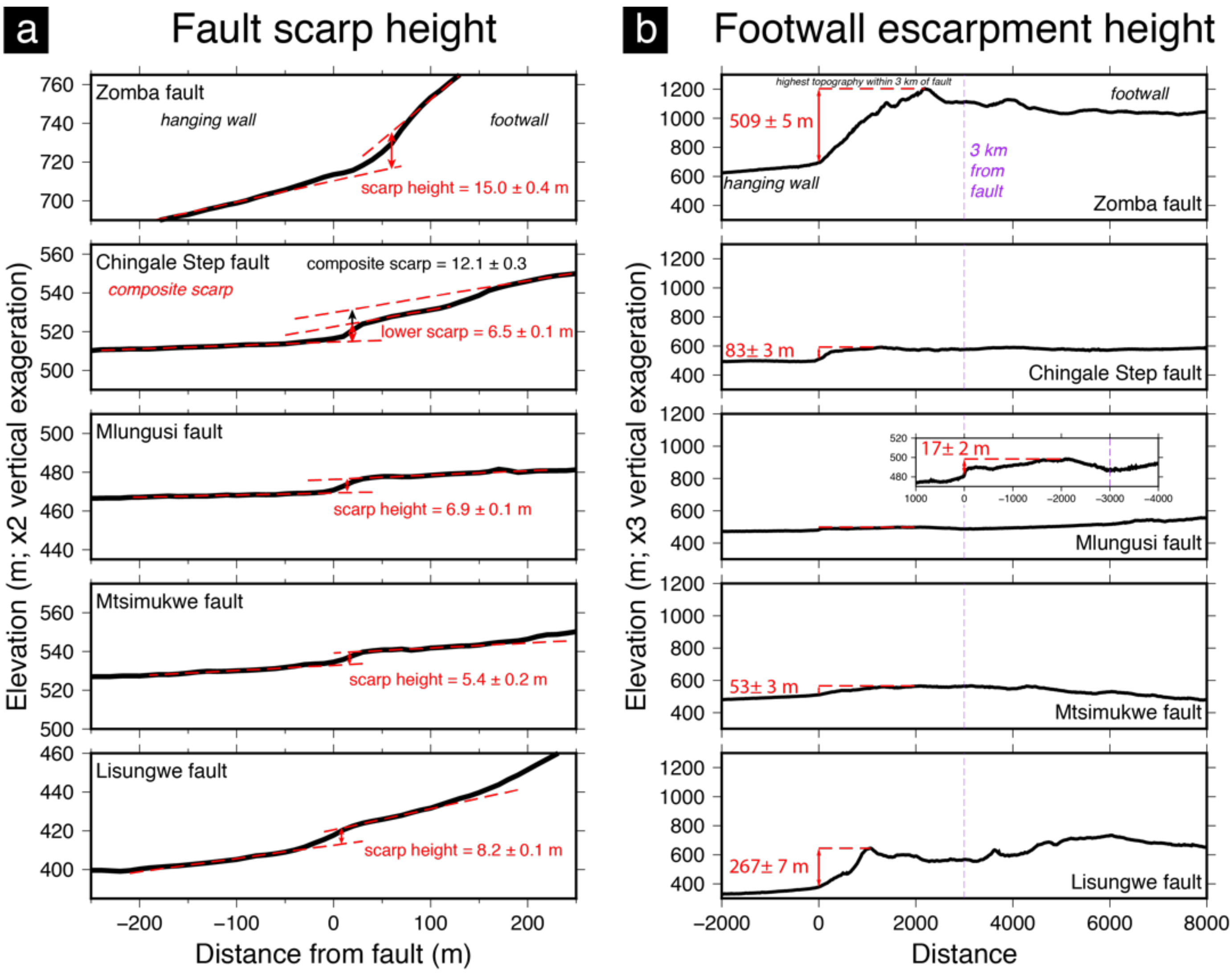

Figure 4: Examples of topographic profiles used to assess fault activity in the Zomba Graben. (a) Example topographic profiles used to calculate the height of the fault scarps in the Zomba Graben. The fault scarps are characterised by locally steep slopes at the base of the larger footwall escarpments. Along the Chingale Step fault, a composite scarp is observed with the lower and upper slopes offset in at least two difference events. For all other, only a single offset was observed. (b) Example of the topographic profile used to calculate the height of the footwall escarpment, which we use as a proxy for minimum throw. The height is measured as the maximum relief within 3 km of the footwall.

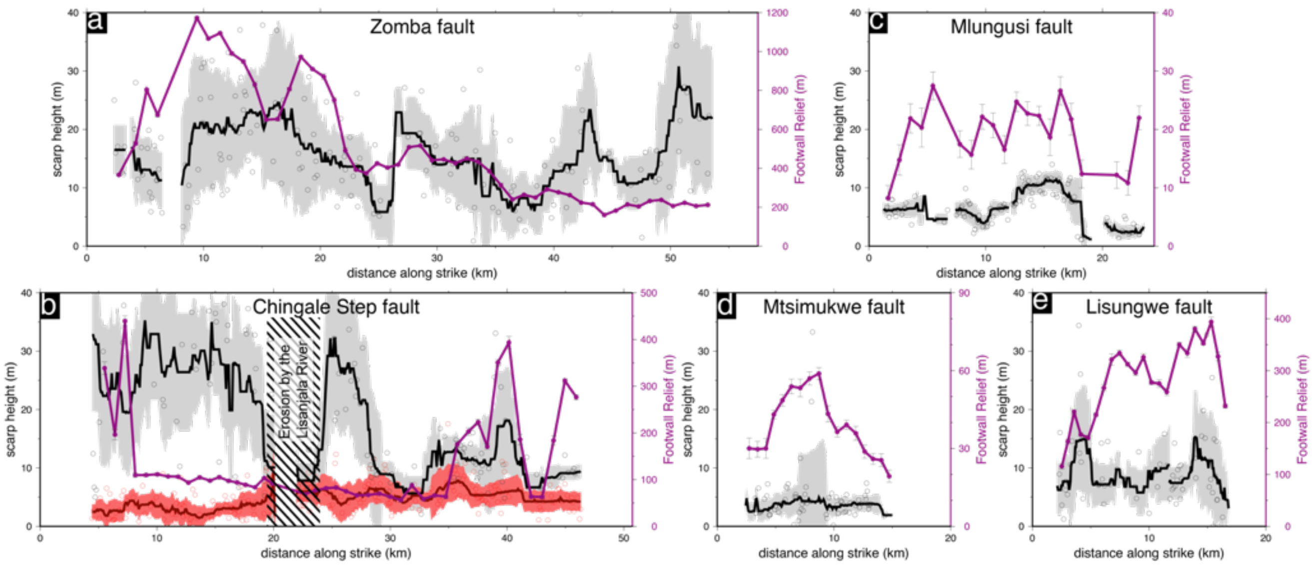

Figure 5: Fault scarp height (black) and footwall escarpment height (purple) for the five faults in the Zomba Graben. Note horizontal and scarp height scales are all equal but footwall relief scales differ in each plot. For the scarp height, the circles show the individual measurements, the solid black lines is the 3 km wide moving median with the 1σ error shaded. (a) The Zomba fault. (b) The Chingale Step fault. The red lines and points indicates the height of the lowest scarp on the composite scarp (see Figure 3 and S2). The black line and points are the height of the composite scarp. The shaded area is where offsets have been eroded by the Lisanjala River. (c) The Mlungusi fault. (d) The Mtsimukwe fault. (e) The Lisungwe fault.

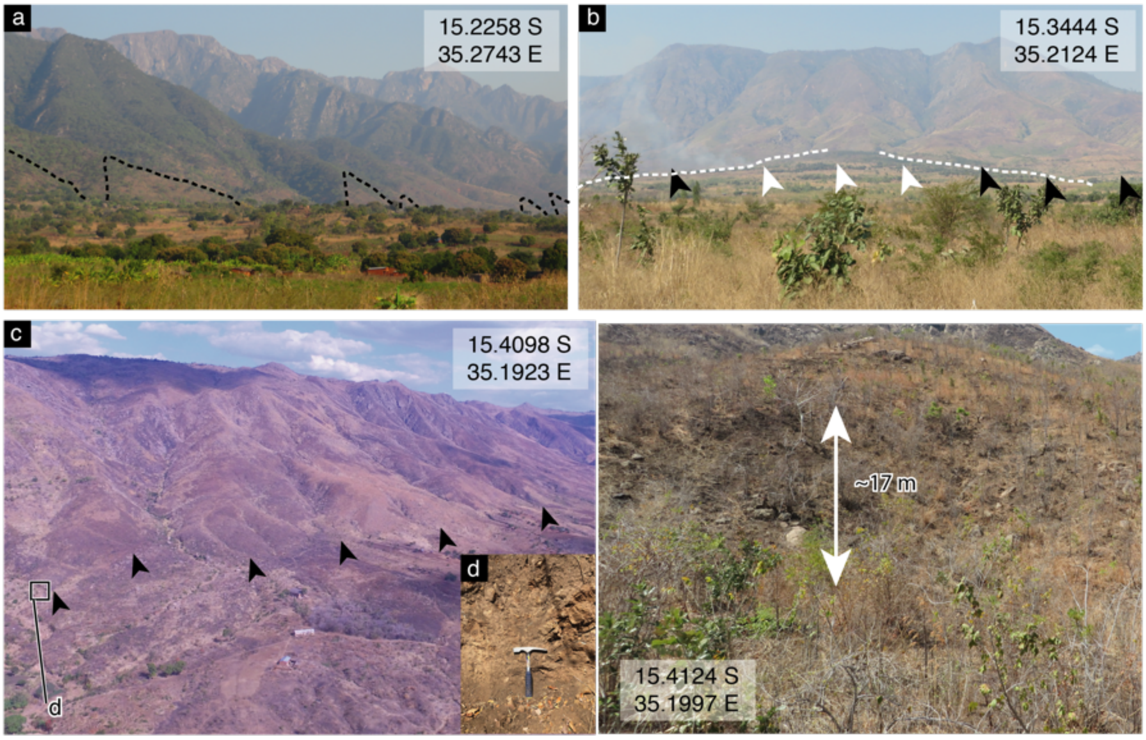

Figure 6: Field observations of the Zomba fault. (a) Triangular facets (black dashed lines) observed at the northern end of the fault. The hangingwall-footwall contact of the facets is not visible in this photo. (b) Alluvial fan observed in the section of the fault where the Zomba plateau is in the footwall of the fault. The black arrows indicate the location of the fault, the white arrows show where the fault crosses and offsets the alluvial fan. The age of the alluvial fan is not known. (c) The fault scarp at the southern end of the Zomba fault (indicated by black arrows). (d) Fractured basement rock consistent with a fault zone observed where exposed in stream beds at the base of the fault scarp. (e) Steep scarp at the base of the footwall escarpment. A scarp height of ~17 m was measured in the field and is consistent with the measurements made using remote sensing data (Figure 5).

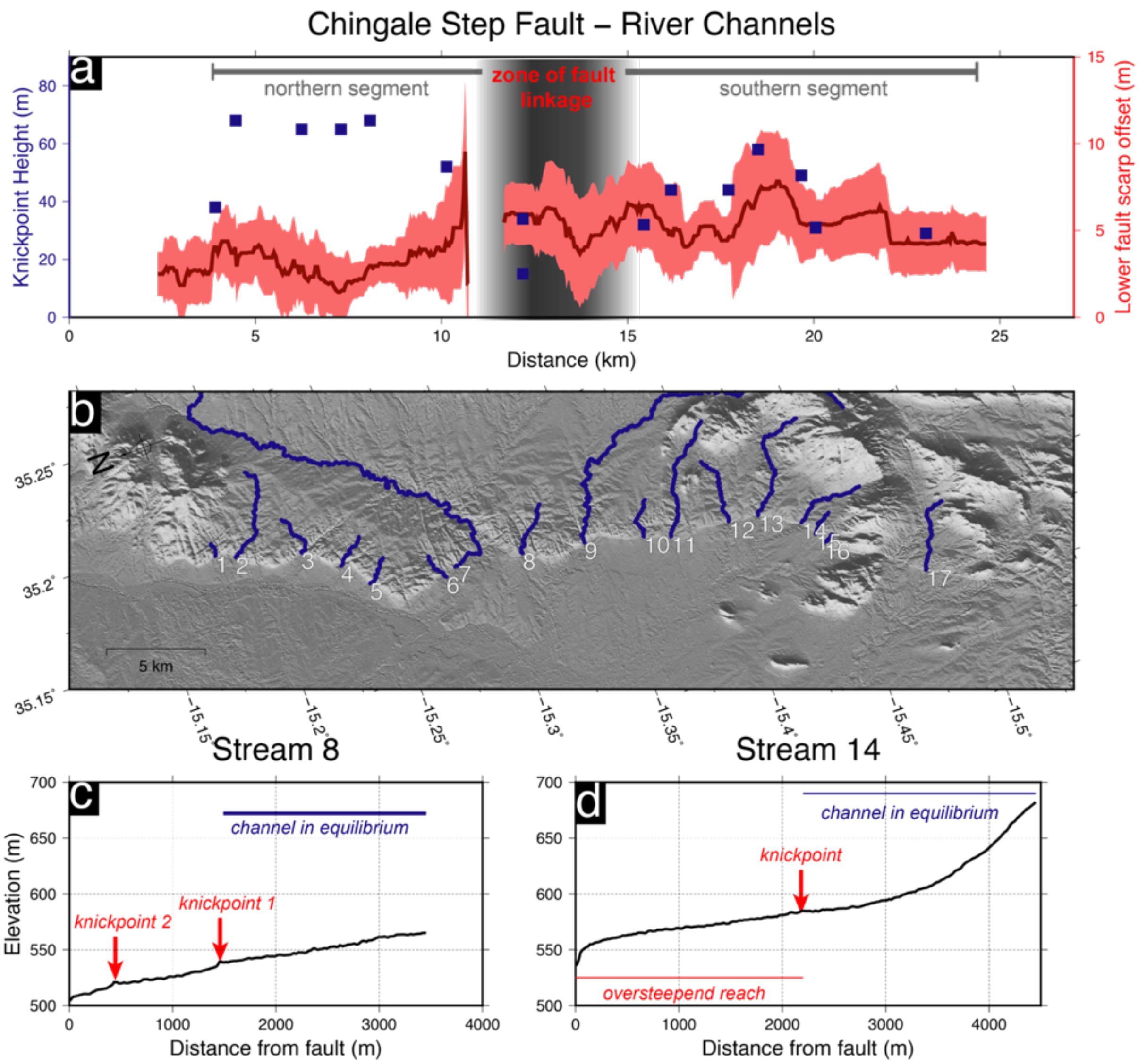

Figure 7: Rivers crossing the Chingale Step fault. (a) The elevation of the knickpoints, at the top of oversteepened portions of the river long profiles (see Figure S3), above the fault scarp (blue squares). Red shows the offset across the lower fault scarp on the Chingale Step Fault (light red is 1 σ error). The gap is due to erosion by the Lisanjala River (stream 7). (b) Map of the footwall river channels that cross the Chingale Step fault. Channels 7 and 9 were not analysed as they both exhibit behaviour which would suggest that they were not detachment limited and both cross multiple lithologies in the footwall of the Chingale Step fault. (c) Stream 8 which is found in the linkage zone between the northern and southern segment of the fault and displays two prominent knickpoints. (d) Stream 14 shows a clear

oversteepened reach in the footwall of the fault. Further upstream the channel is in equilibrium.

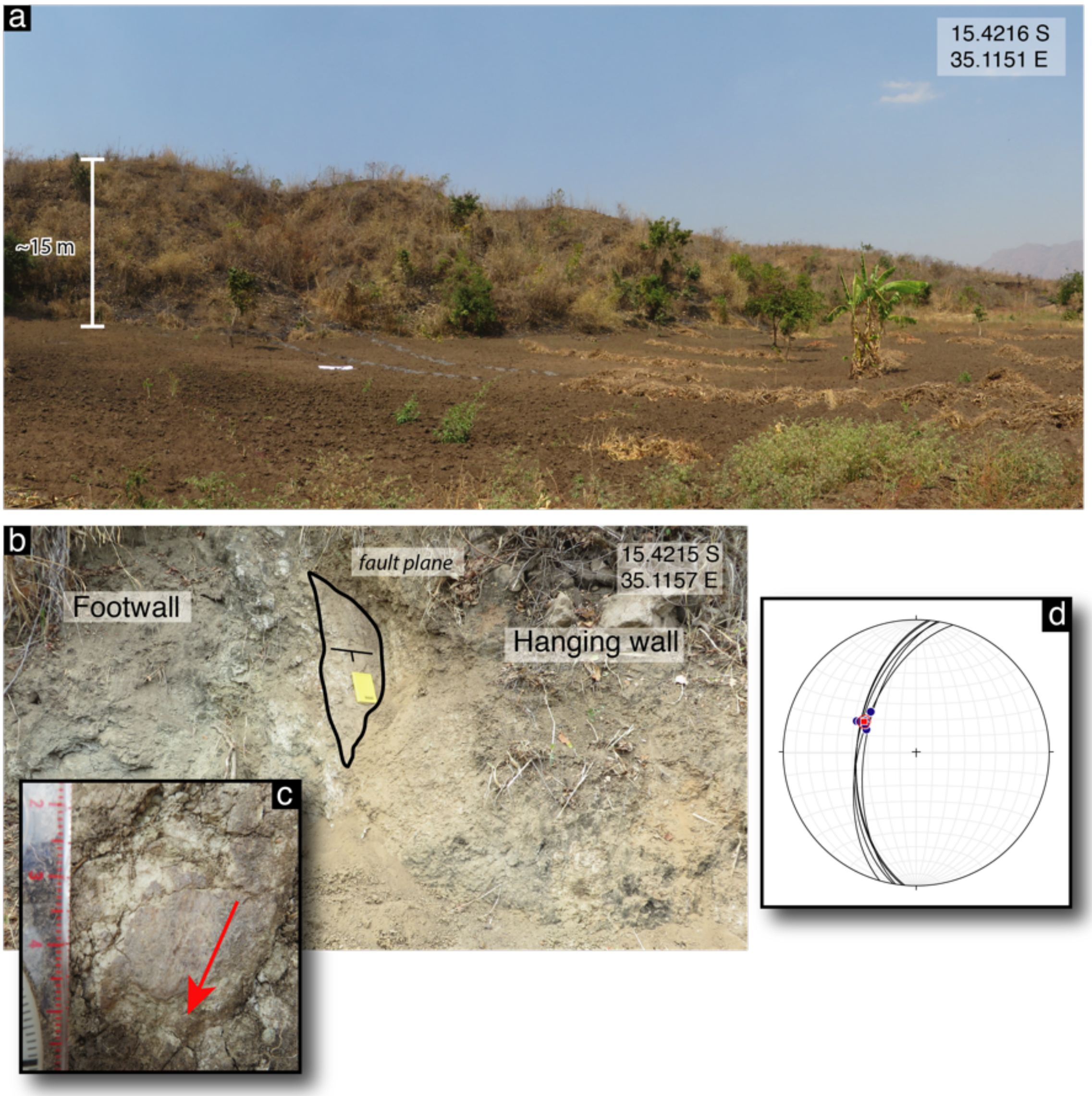

Figure 8. the Chingale Step fault. (a) Fault scarp along the southern section of the Chingale Step fault. The hangingwall is comprised of a mix of fluvial, alluvial and lacustrine deposits whereas bedrock is exposed in the footwall with a thin soil cover. The slickensides shown in part c were observed in a stream bed ~50 m north of this site. (b) The exposure of the fault plane at the Kalira River site. (c) Exposed slickensides measured on a polished fault plane exposed at the side of the river bank. (d) Stereonet showing the fault plane orientation (black lines), the average strike and dip is 189°/54°. The trend and plunge of the slickensides (blue dots) is shown in part b, the average trend and plunge (red dot) is 52° → 301° (N=5).

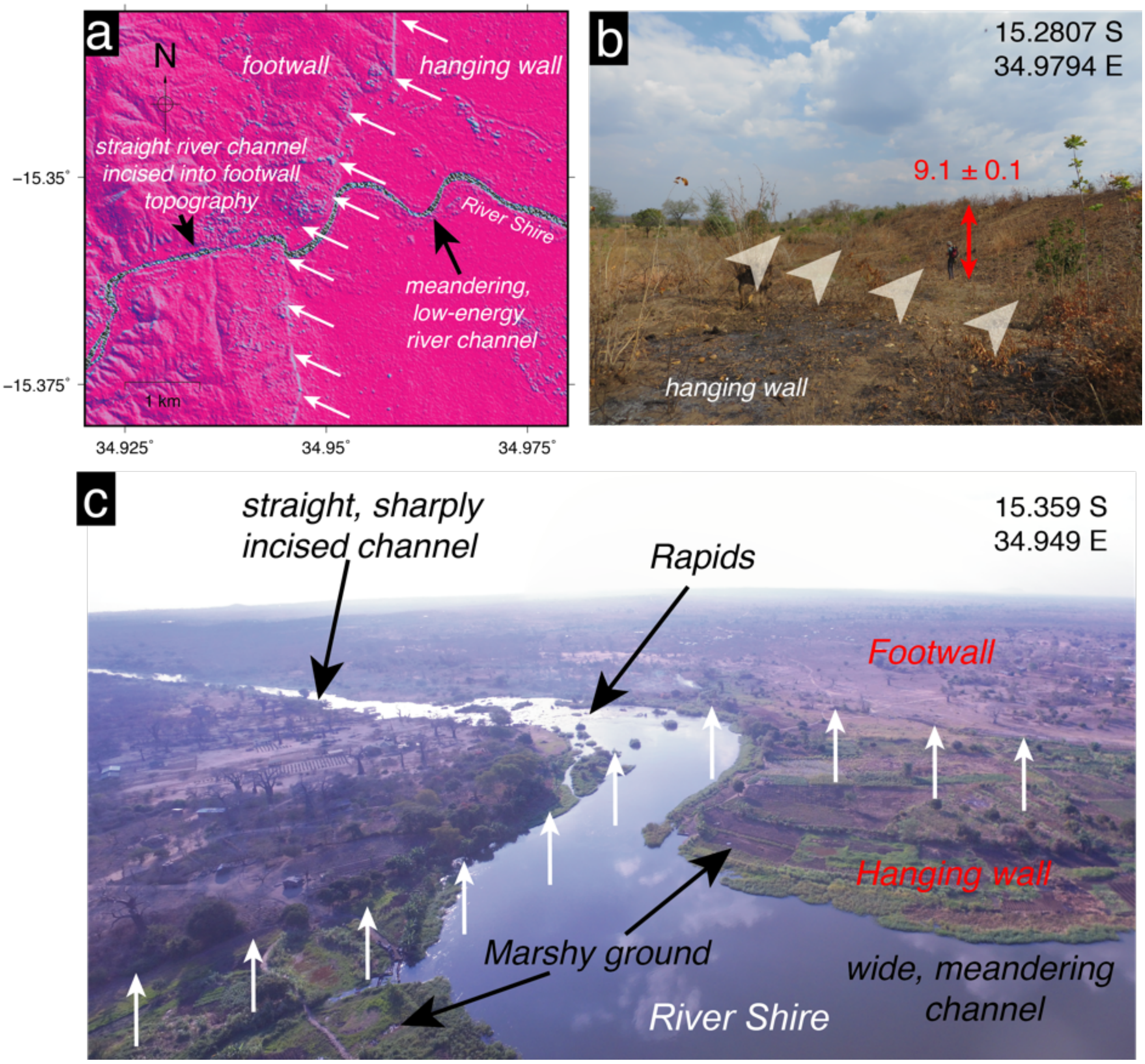

Figure 9: The interaction between the Mlungusi fault and the River Shire. (a) Slope map where the River Shire crosses the Mlungusi fault with the fault scarp indicated by white arrows. (b) The fault scarp formed by the Mlungusi Fault (~3 km to north of parts a and c). The white arrows indicate the base of the fault scarp, the offset is indicated in red. (c) Photo taken from a drone of the location where the River Shire crosses the Mlungusi fault. The location of the scarp is indicated with white arrows.

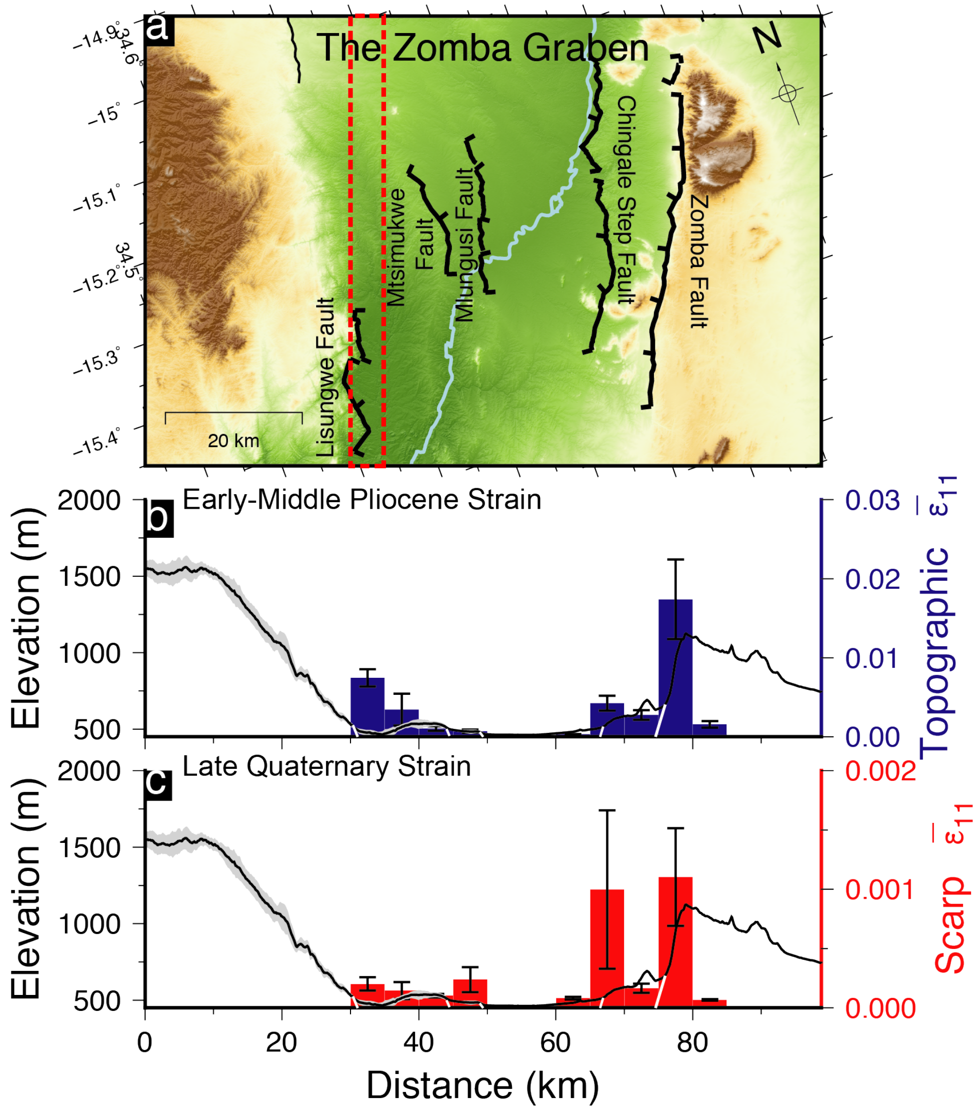

Figure 10: Distribution of strain in the Zomba Graben. (a) Active faults and topography of the Zomba Graben. The active faults analysed in this paper are indicated with thick black lines. ε_{11} direction for parts b-c is horizontal in this projection (projection is rotated 10° to the West). An example of the 5 km width bins used to calculate the strain is shown with the dotted red line. (b) Rift-wide distribution of strain calculated using the footwall relief measurements across each fault in 5 km width areas bins. The length of the bins matches the area shown in part a. The measured offsets are then averaged in each 5km width bin before the strain is calculated in the ε_{11} direction. (c) Rift-wide distribution of strain calculated using the fault scarp offsets measured across each fault in 5km width bins. For

the Chingale Step fault, the total scarp height measurements are used, rather than the height of the lower offset measured at the base of the fault scarp.

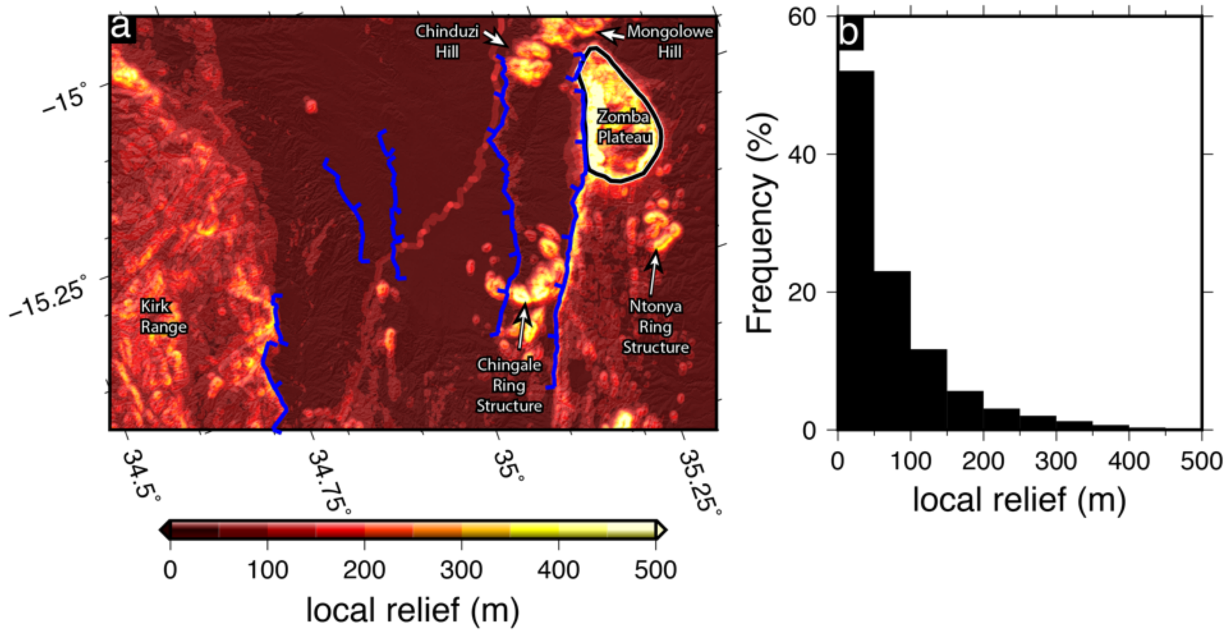

Figure 11: Local relief in the Zomba Graben. (a) Local relief calculated in 1 km sized windows within the Zomba Graben. High values associated with the River Shire are due to errors in the TanDEMx DEM caused by poor coherence of the water in the river which leads to random height errors (Wessel et al., 2018). Prominent zones of high local relief are related to pre-existing topographic features such as the Zomba Plateau, the Ntonya Ring Structure (an intrusion of similar age to the Chingale Ring Structure), the Kirk Range and the Chingale Ring Structure. The Chinduzi and Mongolowe hills are syenite-granite intrusion of the Chilwa Alkaline province (the same age as the Zomba Plateau). (b) Histogram of local relief values in the Zomba Graben (calculated using the area and data shown in part a).

Table 1: The Geometry, activity rates and strain across faults in the Zomba Graben.

Fault	Length (km)	Strike(°)	Dip Direction	Mean Scarp height (m)	Mean Footwall Relief (m)	% of Total Strain	% of late-Quaternary strain
Zomba	51	025	West	15.6 ± 5.2	326 ± 113	56 ± 16	43 ± 15
Chingale Step	39	022	West	19.6 ± 12.1	84 ± 18	12 ± 2	35 ± 22
Mlungusi	22	013	East	6.9 ± 3.1	19 ± 5	2 ± 0	8 ± 3
Mtsimukwe	13	177	East	3.6 ± 0.7	38 ± 12	11 ± 6	8 ± 3
Lisungwe	23	019	East	10.0 ± 6.7	277 ± 76	19 ± 3	6 ± 2